

https://dspace.org/

Review of channel estimation for candidate waveforms of next generation networks.

Ijiga, O.E.; Ogundile, O.O.; Familua, A.D.; Versfeld, D.J.J.

2019-09
MDPI
https://hdl.handle.net/10539/28451
Ijiga, O.E. et.al. 2019. Review of channel estimation for candidate waveforms of next generation networks. Electronics 8(9), Article number 956. DOI: 10.3390/electronics8090956

Downloaded from a DSpace repository. https://dspace.org/

electronics

MDPI

Review

Review of Channel Estimation for Candidate Waveforms of Next Generation Networks

Owoicho E. Ijiga [1,*], Olayinka O. Ogundile [2], Ayokunle D. Familua [3] and Daniel J. J. Versfeld [2]

[1] School of Electrical and Information Engineering, University of the Witwatersrand, Johannesburg 2000, South Africa

[2] Department of Electrical and Electronics Engineering, Stellenbosch University, Stellenbosch 7602, South Africa

[3] Center for Telecommunications, Department of Electrical and Electronics Engineering Science, University of Johannesburg, Johannesburg 2006, South Africa

* Correspondence: owoicho.ijiga@gmail.com

Received: 14 July 2019; Accepted: 15 August 2019; Published: 29 August 2019



Abstract: The advancement in wireless communication applications encourages the use of effective and efficient channel estimation (CE) techniques because of the varying behaviour of the Rayleigh fading channel. In most cases, the emphasis of most proposed CE schemes is to improve the CE performance and complexity for ensuring quality signal reception and improved system throughput. Candidate waveforms whose designs are based on filter bank multi-carrier (FBMC) modulation techniques such as filter bank orthogonal frequency division multiplexing based on offset quadrature amplitude modulation (OFDM-OQAM), universal filtered multicarrier (UFMC) and generalised frequency division multiplexing based on offset quadrature amplitude modulation (GFDM-OQAM) are no exception to the use of these proposed CE techniques in the literature. These schemes are considered as potential waveform candidates for the physical/media access control layer of the emerging fifth generation (5G) networks. Therefore, pinpoint CE techniques represent an important requirement for these waveforms to attain their full potentials. In this regard, this paper reviews the concept of CE as applicable to these waveforms as well as other waveform candidates under consideration in the emerging 5G networks. Since the design of the majority of the waveform candidates is filter based, a review of the general filter design considerations is presented in this paper. Secondly, we review general CE techniques for candidate waveforms of next generation networks and classify some of the studied CE techniques. In particular, we classify the CE schemes used in filter bank OFDM-OQAM and GFDM-OQAM based transceivers and present a performance comparison of some of these CE schemes. Besides, the paper reviews the performances of two linear CE schemes and three adaptive based CE schemes for two FBMC based waveform candidates assuming near perfect reconstruction (NPR) and non-perfect reconstruction (Non-PR) filter designs over slow and fast frequency selective Rayleigh fading channels. The results obtained are documented through computer simulations, where the performances of the studied CE schemes in terms of the normalised mean square error (NMSE) are analysed. Lastly, we summarise the findings of this work and suggest possible research directions in order to improve the potentials of the studied candidate waveforms over Rayleigh fading channels.

Keywords: filter bank; Non-PR; NPR; channel estimation; next generation networks; 5G waveforms; channel fading

1. Introduction

The speedy growth of wireless communication in recent years has placed a huge demand on the available frequency spectrum, making this resource a scarce commodity [1,2]. The concept of

multi-carrier modulation (MCM) is usually adopted in modern communication systems so as to ensure efficient utilisation of the scarce frequency spectrum and yield higher system throughput. In MCM technologies, wideband signals are split at high symbol rate into multiple lower rate signals, where the low rate signals are modulated onto narrowband orthogonal sub-channels (sub-carriers) for the simultaneous transmission of data over the wireless channel [3]. MCM schemes offer more benefits than their single carrier modulation (SCM) counterparts. One benefit of MCM schemes over SCM schemes is in their ability to offer higher spectral efficiency mainly due to the channel division as well as overlapping of the orthogonal sub-carriers. For efficient sharing of the scare frequency spectrum and for higher data rate applications, several wireless channel access methods have been developed over the years. Multiple access methods provide an efficient way for several communication users to effectively share the same spectrum resource without causing interference with one another.

In wireless networks, these access schemes are generally divided into two basic groups: contention-free channel access schemes and contention-based random channel access schemes [4,5]. In contention-free access schemes, a central entity allocates several nodes using radio resources such as time slots, frequency and code, where data are transmitted through these nodes by the use of the allocated radio resource. Examples of contention-free channel access schemes include frequency division multiple access (FDMA), time division multiple access (TDMA) and code division multiple access (CDMA) schemes. On the other hand, the nodes in contention-based random channel access schemes compete with one another for the transmission of data over the wireless channel. The data in contention-based random channel access schemes are usually received without collision. Carrier sense multiple access (CSMA) and Aloha method are examples of the contention-based random channel access schemes.

In FDMA schemes, each user is allocated a frequency channel where they can transmit their respective signals at the same time over the available spectrum resource while multiple users are allowed to transmit their signals at the same frequency over the available frequency spectrum at different time slots in TDMA schemes. CDMA schemes are multiple access technologies that allow multiple users to simultaneously and asynchronously access a spectrum resource by modulating and spreading their information signals with pre-assigned signature codes or spreading codes which are orthogonal to one another [6]. CDMA offers several advantages over FDMA and TDMA such as improvement in spectral efficiency, larger system capacity, higher security and better anti-interference ability [7]. The first to the third generation of wireless networks is built based on the contention-free channel access schemes. The first generation (1G) of wireless networks became operational in 1979 [7]. It is known as analogue cellular systems because the design of these cellular systems is based on FDMA and analogue frequency modulation technology. The second generation (2G) of wireless systems is designed based on either TDMA or CDMA technology while the third generation (3G) of wireless networks is based on CDMA, where air interface standards such as wideband-CDMA (WCDMA), CMDA 2000 and time division synchronous CDMA (TD-SCDMA) were developed.

In recent decade, an improved version of FDMA scheme has been proposed and developed to offer higher data rates, improved spectral efficiency and better anti-interference ability. This access scheme is known as orthogonal frequency division multiple access (OFDMA) with cyclic prefix (CP). The scheme addresses the problem of bandwidth wastage encountered in FDMA schemes by the overlapping of the orthogonal sub-channels [3,8]. The introduced CP in this scheme is used to offer robustness against the harmful effects of multipath fading and it is usually implemented based on inverse fast Fourier transform/fast Fourier transform (IFFT/FFT) [9]. Due to these improvements, the CP based OFDMA (CP-OFDMA) scheme is recommended as the main multiple access method for the fourth generation (4G) of mobile networks, which is designed based on the long-term evolution (LTE) standards for wireless broadband communication systems.

Despite the improvements of the CP based orthogonal frequency division multiplexing (OFDM) technology, it is not considered as the most promising multiplexing scheme for the neXt generation (xG) of wireless networks which is the emerging fifth generation (5G) networks. It is proposed

that the emerging 5G wireless networks be designed using filter bank multi-carrier (FBMC) based transceivers. FBMC based schemes with offset quadrature amplitude modulation (FBMC-OQAM) provide an alternative modulation scheme that limits the shortcomings of CP-OFDM systems by the elimination of CP; hence, resulting in higher system spectral efficiency and provision of enhanced robustness to synchronisation errors [10]. Various FBMC systems have been considered as potential waveforms for the emerging 5G networks of wireless systems and beyond. These include filter bank orthogonal frequency division multiplexing with offset quadrature amplitude modulation (OFDM-OQAM) [11,12], universal filtered multi-carrier (UFMC) [13,14], bi-orthogonal frequency division multiplexing (BFDM) [15,16] and generalised frequency division multiplexing (GFDM) [17,18]. The concept of perfect reconstruction (PR) or near perfect reconstruction (NPR) is used to design the aforementioned FBMC waveforms where well-designed prototype filters are used to design the synthesis and analysis filter banks of these FBMC based transceivers. This concept either replaces or minimises the CP usage that is common to CP-OFDM of the 4G networks; thus, providing higher spectral efficiencies and data rate improvement.

The transmitted symbols of a baseband signal are usually corrupted by noise as they propagate through the communication channel. They experience detrimental effects such as multipath propagation and fading which eventually makes it difficult for accurate detection of the transmitted symbols. For accurate detection of the transmitted symbols, pinpoint channel estimation (CE) is required [19,20]. Channel estimation makes it possible for the receiver to approximate the channel impulse response (CIR) of the communication channel and to predict/understand the effects of the communication channel on the transmitted symbols. This is required for perfect reconstruction of the transmitted symbols. Several CE algorithms have been proposed in the literature for general wireless communication systems. This paper reviews and classifies the CE schemes in the literature. In particular, an overview of the CE schemes adopted in the literature for filter bank multi-carrier based systems is presented, where we classify the CE schemes used in filter bank OFDM-OQAM and GFDM-OQAM transceivers. Moreover, the paper reviews the performances of two linear CE schemes and three adaptive CE schemes for the two aforementioned FBMC-based waveforms assuming near perfect reconstruction (NPR) and non-perfect reconstruction (Non-PR) filter designs over slow and fast frequency selective Rayleigh fading channels. Note that, to efficiently review the performances of these CE schemes, we present a step-wise system description and implementation of the filter bank OFDM-OQAM and GFDM-OQAM FBMC-based transceiver. In addition, since the designs of these FBMC transceivers are based on filters, we firstly present a review of the filter design in Section 2.

The contribution and relevance of this paper are as follows. This paper is important in general for wireless communication systems and the emerging 5G networks and beyond. The paper presents a detailed and up-to-date review of the basic concepts of CE with respect to non-filtered based waveforms and with particular reference to two filter bank multi-carrier based waveforms that are currently being considered as potential candidates for the physical layer design of the emerging next generation of wireless networks. Furthermore, the paper presents a step-wise system description, implementation and performance analysis of relevant CE schemes used in the FBMC-based transceiver. In this case, researchers and practitioners in this field can perceive the different CE schemes in order to make useful decisions based on their application requirements. Finally, this review presents possible research directions in order for FBMC schemes to attain its full potentials over Rayleigh fading channels. Although there are other fading channels such as the Nakagami fading channel and the Rician fading channel, we centre our attention on the Rayleigh fading channel model because it is the most common and realistic channel to model a wireless communication link [21].

The remainder of this paper is structured as follows. Section 2 describes the general structure of FBMC systems which is adopted for designing the FBMC-OQAM waveforms in this paper. The fundamentals of CE and its application to filter bank OFDM-OQAM and GFDM-OQAM is presented in Section 3. A system model description of both FBMC-OQAM waveforms is presented in Section 4 assuming both NPR and Non-PR. In Section 5, the simulation results of the analysed CE

schemes are presented. In Section 6, we summarise the findings of this work and suggest possible research directions. Lastly, Section 7 concludes the paper.

2. Structure of Filter Bank Multi-Carrier Systems

One of the most fundamental building blocks of filter bank multi-carrier waveforms is a well-designed prototype filter. Therefore, this section presents a review of the filters and the fundamental building block of FBMC based transceivers. A filter can be defined as a frequency selective circuit that is designed to pass signals of a particular frequency band while attenuating signals of other frequencies [22]. Filters are generally employed to eliminate or minimise unwanted system features such as interference, noise and distortions. Filters are classified in many ways, which could depend on the functions they are required to perform or be based on their physical structures. Hence, filters may be broadly classified as analogue/digital filters (based on function), active/passive filters (based on structure), etc. Passive filters are filters that are designed with the use of passive components such as resistors, capacitors, inductors, relays, etc. Active filters are designed with the aid of active components such as transistors, integrated circuits, diodes and passive components.

Digital filters also known as discrete-time filters are employed in digital signal processing (DSP), mainly for the separation of digital signals that are combined together and for the restoration of distorted signals. The implementation of digital filters can be realised by convolution or by recursion. Convolution filters are known as finite impulse response (FIR) filters while recursion filters are known as infinite impulse response (IIR) filters. An FIR filter is a digital filter that has a finite duration of impulse response. These filters are reverse cases of the IIR filters since there is no feedback of output signals into the input. As such, they can be called non-recursive filters [22,23]. The impulse responses of these filters are finite because of the absence of feedback. Some of the methods used for designing FIR filters include windowing, frequency sampling and equiripple approximation [22,24]. The finite length impulse response of the FIR filters is obtained by truncating an infinite length impulse response. The truncation of an infinite duration sequence to yield a finite response is termed windowing. Some functions are used to perform windowing. Examples of such functions include rectangular, Barlett, Hanning, Hamming and Blackman windowing functions. Infinite impulse response filters are digital filters that have an infinite duration of impulse response. They are also called recursive filters because they are designed to use the feedback signals obtained from the system output. These types of filters have nonlinear phase and are usually unstable. Some examples of these filters are Butterworth filters, Chebyshev type I and Chebyshev type II filters, Elliptic filters and Bessel filters. Other examples of this kind of filters are described in [22,23].

All filters are classified based on their frequency response characteristics [22,25]. In the design of digital filters, the frequencies that are allowed to pass through are known as pass-band frequencies [25], whereas the rejected frequencies can be referred to as the stop-band frequencies. Based on this information, filters are classified as low-pass filters, high-pass filters, band-pass filters, band-stop filters (band-reject filters) and the all-pass filters. Low-pass filters allow signals of low frequencies to pass through while rejecting signals above its cut-off frequency. High-pass filters eliminate frequencies below its cut-off frequency while allowing signals of high frequencies to pass through. Band-pass filters allow signals within a certain range of frequencies to pass through while attenuating all other frequencies. Band-stop filters allow all frequencies to pass through while attenuating a certain range of frequencies. Finally, the all-pass filters allow all frequencies to pass through; however, they change the phase of the passing signals without changing their amplitudes. The structure of FIR filters consist of series of multipliers, delays and adders coupled together to give an output. This design makes these filters suitable for designing multirate filters. Multirate filtering constitutes the fundamental building block of FBMC systems. An overview of multirate filtering is presented in Section 2.1.

2.1. Multirate Filtering

One basic notion that is adopted in DSP is the concept of sampling rate [26]. Sampling rate involves the conversion of a signal from a given rate to a different rate. It is worth noting that systems that adopt multiple sampling rates in DSP are known as multirate digital signal processing systems. These systems employ the use of multirate filters which are classified into hybrid and polyphase filters. Polyphase filters have demonstrated good performances over the years, therefore proving to be an excellent multirate filter that can be effectively adopted to solve wireless communication problems [26]. Multirate filters find useful applications in digital audio and video processing, speech coding, image compression, adaptive signal processing, scrambling, software define radios and modern DSP systems [26–28]. Multirate Filtering is based on two filtering techniques: decimation and interpolation [28,29].

Interpolation is a sampling rate conversion technique that is adopted to remove the effects of imaging through the use of an interpolation filter while increasing the sampling rate of the signal using an interpolator (upsampler). Upsampling is used to increase the sampling rate of a signal by the insertion of an integral number of samples (zeros) between consecutive samples of input signals. Figure 1a shows a simple diagrammatic representation of an interpolation process that consist of an upsampler/expander of factor M and an interpolation filter with response $g[\dot{n}, k]$. In this figure, $y[\dot{n}, k]$ represents the higher rate output symbols that are received after upsampling process while $x[n, k]$ represents the input symbols at time n and sub-carrier k. The output time index $\dot{n}$ is at a higher rate in comparison to the input index n. This process of interpolation/signal rate conversion is illustrated in Figure 2, where the sampling rate of Figure 2b is increased in comparison to the sampling rate of Figure 2a, by the insertion of zeros between consecutive samples. On the other hand, decimation is a sampling rate conversion technique that is usually adopted at the receiver of a communication system to suppress aliasing by the use of a decimation filter and a downsampler [30]. In addition, they are used to reduce the sampling rate of a signal by a factor M as shown in Figure 1b. Similar to Figure 2, the decimation process is shown in Figure 3.

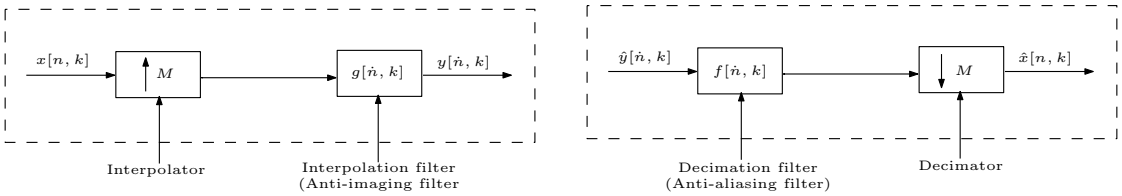

(**a**) Interpolation (**b**) Decimation

Figure 1. Structure of multirate filtering.

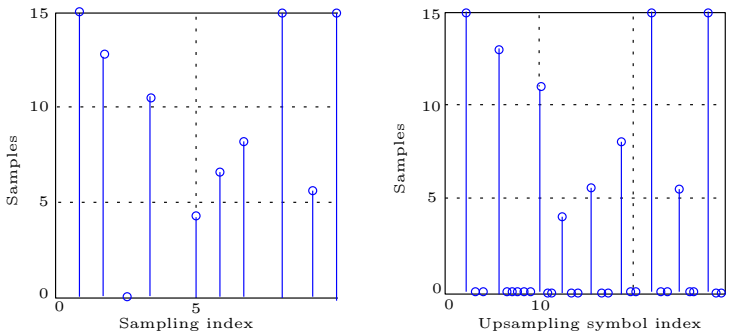

(**a**) (**b**)

Figure 2. Time domain plot of signal interpolation for $M = 2$. (**a**) Before upsampling. (**b**) After upsampling.

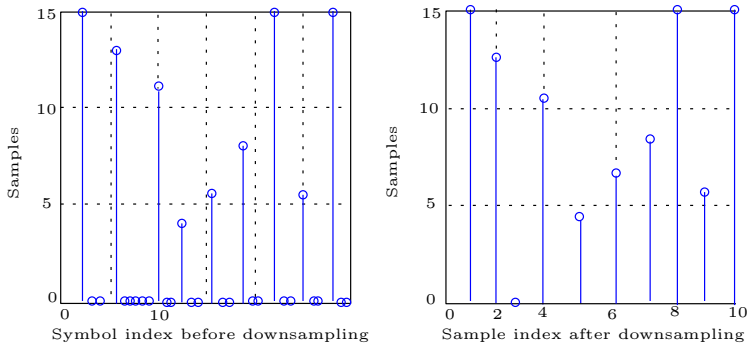

Figure 3. Time domain plot of signal decimation for $M = 2$.

2.2. Design of Multirate Filters: Polyphase Filters

In designing an FBMC system, the first step is to design a low-pass prototype filter that meets the requirements of NPR or PR. In [31], three kinds of prototype filters are analysed and compared for the design of FBMC based systems. The authors proposed a prototype filter model called Farhang which offers the best performance in terms of sidelobe suppression in comparison to the widely used square-root raised-cosine (SRRC) filter, as well as the discrete-time square root Nyquist filter model designed in [32]. The prototype filters are adopted for designing interpolation and decimation filters. Above, we show in Figure 1a the basic structure of implementing interpolation in FBMC systems. This figure can be extended to form the basic structure of interpolation in polyphase filter banks over M sub-carriers, as depicted in Figure 4a [33]. The discrete, real input signal $x[n,k]$ of Figure 1a is split to yield M sub-band signals by the use of synthesis band-pass filters whose impulse response is given as $g[\dot{n},k]$ in order to realise the polyphase representation shown in Figure 4a. Similarly, Figure 1b shows the process of decimation in multirate systems that are usually adopted for combating the effects of aliasing. This figure can be used as a foundation to develop an efficient implementation structure for polyphase decimation as shown in Figure 4b.

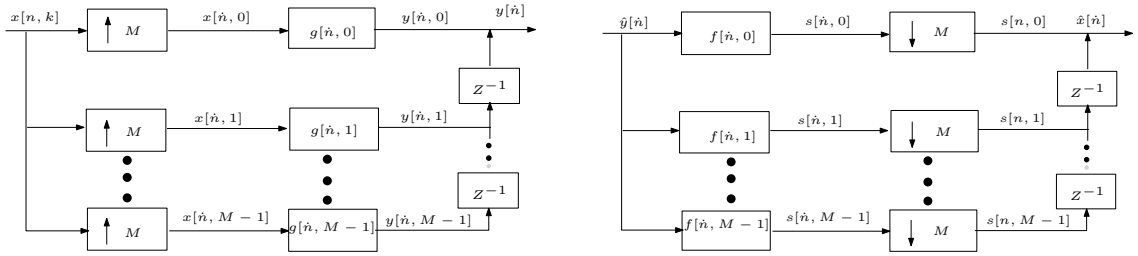

(**a**) Interpolation (**b**) Decimation

Figure 4. Basic structure of polyphase filters.

2.3. Basic Structure of FBMC Systems

Digital filter bank multi-carrier based transceivers are made up of two filter banks: synthesis filter bank (SFB) and analysis filter bank (AFB) [22,24]. The synthesis filter bank is positioned at the transmitter while the analysis filter bank is found at the receiver. It is designed with M digital filters arranged in a parallel configuration [22,24]. The synthesis filter combines M signals at the transmitter into a single signal that is ready for transmission over a channel. This single signal can also be referred to as the reconstructed signal. In PR filter banks, the output signal is a delayed replica of the input signal [34]. In practical applications, the output signal is designed to achieve NPR. As in the design of decimation and interpolation filters discussed in Section 2.1, the synthesis filter bank is designed with an interpolation filter and an upsampler, while the analysis filter is designed with a decimation filter and a downsampler. This makes the multirate filters periodically linear time-varying systems because they are made up of linear filters and also perform time-varying linear operations such as decimation [35]. Figure 5 illustrates a basic structure of digital filter banks [10,36].

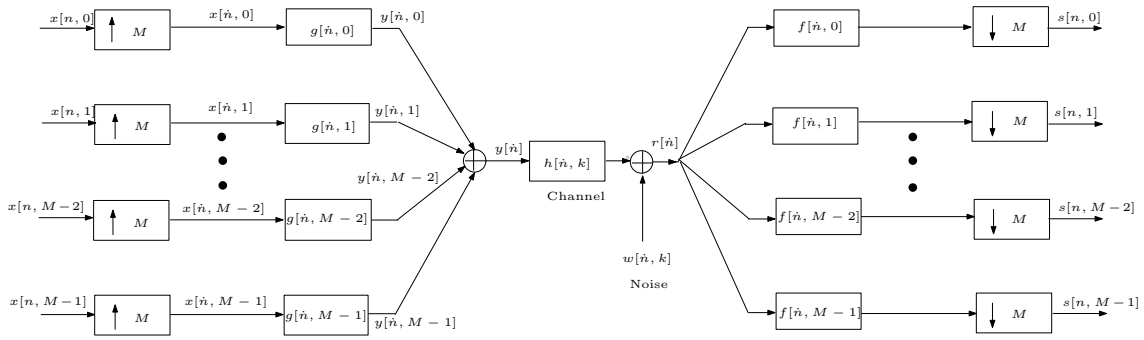

Figure 5. Basic structure of FBMC based transceivers.

This structure is considered as an FBMC system because it is designed to offer multirate filtering where the sampling rate of the input symbols $x[n,k]$ at the transmitter is increased using an interpolator. Subsequently, it is filtered with a low-pass anti-imaging filter $g[\dot{n},k]$ so as to remove images of the input spectrum. In other words, this system is adopted to connect and transmit the input symbols $(x[n,k])$ over the fading channel by converting the symbols into higher rates using an SFB. This enhances efficient data transmission over the frequency selective multipath fading channel in comparison with single rate multi-carrier systems. The upsampling of the input symbols at the SFB is performed in order to ensure that the sampling rate of the signals at the receiver input is the same, which is subsequently decimated at the AFB by filtering the received signals with the aid of an anti-aliasing filter $(f[\dot{n},k])$. The anti-aliasing filter is adopted so as to combat aliasing. The signal is then appropriately downsampled to obtain $\hat{x}[n,k]$ in order to ensure efficient demodulation/detection of the received symbols.

The concepts in Figure 4a,b are combined via a communication channel to realise the general structure of FBMC systems shown in Figure 5. One effective way of implementing FBMC based schemes assuming NPR is by realising the system through the use of discrete Fourier transform (DFT) based polyphase filter bank model, where IFFT is used to transform the input signal from the frequency domain to the time domain. These concepts are combined for the design of the FBMC based transceivers shown in subsequent sections.

Potential FBMC waveforms for 5G networks include filter bank OFDM-OQAM, UFMC [13], BFDM [15,16], and GFDM [37]. These waveforms can be designed using FBMC structures, such as exponentially or cosine modulated filter banks. The aforementioned FBMC transmission waveforms are usually designed based on DFT. Hence, they are classified as DFT based FBMC systems. Other FBMC transmission technologies include discrete wavelet multitone (DWMT) [27,28], filtered multitone (FMT) [9] and cosine modulated multitones [38]. The technologies in [9,27,28,38] are designed based on discrete wavelet transforms (DWT). Accordingly, we classify the FBMC schemes based on the modulation type in Figure 6.

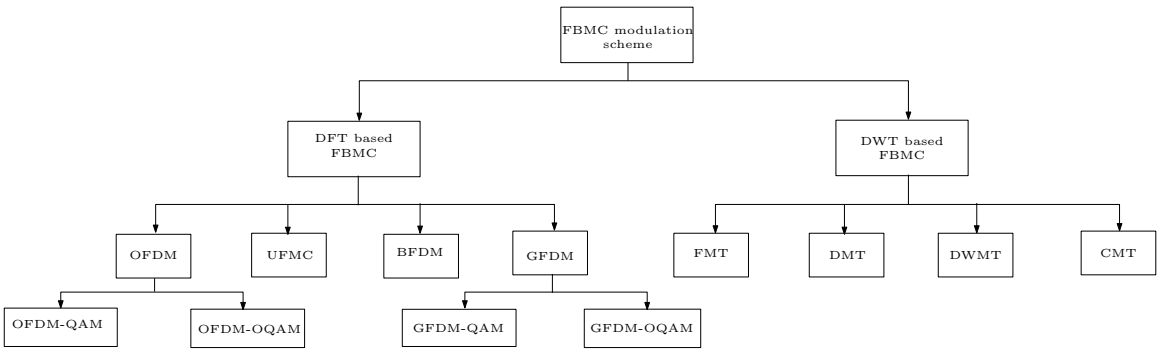

Figure 6. Classification of FBMC schemes based on modulation.

Unlike the DFT based FBMC systems, the DWT based FBMC systems employ the use of wavelet packet transforms (WPT). In wavelet transform, a particular signal of interest is decomposed into a set of waveforms known as wavelets [39]. When DWT is employed, two sets of function associated with low-pass and high-pass filtering are incorporated [39]. In this system, the time domain signal is decomposed into different frequency bands using high-pass and low-pass filters. The incoming signal is passed through a half-band high-pass filter and a half-band low-pass filter, where the former removes all frequencies below half of the highest frequency of incoming signal and the latter remove frequencies that are below half of the highest frequency of the incoming signal [39].

As shown in Figure 6, OFDM-QAM is an FBMC system based on DFT, while DWMT is an FBMC system based on DWT [40]. Their respective transceiver structures are very similar except that DFT is used for transformation in the receiver of the former while DWT is adopted for transformation in the latter. Inverse DFT (IDFT) and inverse DWT (IDWT) are implemented in their respective transmitters. The low-pass FIR prototype synthesis and analysis filters of the FBMC schemes mentioned in Figure 6 (for both DFT and DWT based FBMC systems) can be implemented using various FBMC structures such as exponentially modulated filter banks (EMFB) [41], cosine modulated filter banks (CMFB) [42,43], modified discrete Fourier transform (MDFT) [44] and extended lapped transforms (ELT) [45].

2.4. Overview of Next Generation Networks (5G)

The Cisco Internet Business Solutions Group (IBSG) in 2011 predicted that the number of Internet connected devices will rise to about 50 billion by 2020 [46]. To achieve higher data transmission rates and capacity enhancement due to the high demands of the sparsely available frequency spectrum of wireless communication networks, the downlink layer of the 4G/LTE based system is well designed using OFDMA technology. The use of CP-OFDM in the design of 4G networks offer several benefits, such as improvement in bandwidth/spectrum utilisation (spectral efficiency), robustness to the detrimental effects of multipath fading and efficient frequency domain allocation of available resources/spectrum for enhancement in multiple user (MU) transmissions. However, the 4G CP-OFDM scheme is known to have certain limitations such as introduction of system overhead, sensitivity carrier frequency/time offsets (CFTO) and very high peak-to-average-power ratio (PAPR) [47]. The added system overhead arises from the inclusion of CP in other to combat the effects of multipath propagation as the signal propagates over the wireless frequency selective fading channel. This resulting overhead (from the added CP) reduces system spectral efficiency while CFTO introduces unpleasant ICI due to loss in sub-carrier orthogonality. PAPR [48,49] is the ratio between the maximum power of a sample in an OFDM transmit symbol to the average power of that OFDM symbol. A high PAPR (as characterised by OFDM systems) decreases the efficiency of high power amplifiers and consequently leads to further degradation of system performances. To improve the limitations of the 4G/LTE CP-OFDM system, the xG (5G and beyond) wireless networks are designed to meet fundamental requirements such as very high reliability and robustness, low out-of-band (OOB) emission, ultra-low latency and immensely high data rate capacity [50–52]. We discuss the potential candidates that constitute the air interface configuration for the physical (PHY) and medium access control (MAC) layer of 5G networks in Section 2.4.1. Subsequently, we classify these candidate waveforms in Section 2.4.2.

2.4.1. PHY/MAC Layer Design Considerations for 5G

Three broad application categories are used for characterising 5G wireless communication systems. These categories include: enhanced mobile broadband (eMBB), massive machine type communication (mMTC) and ultra-reliable and low latency communications (URLLC). In cellular networks, eMBB is considered for enhancing spectral efficiency of emerging networks as network end users have insatiable demands for mobile data. Machine type communication (MTC), on the other hand, is an advanced model proposed by the 3rd generation partnership project (3GPP), where electronic devices and machines are configured to efficiently communicate with one another by the transfer of data over wireless communication networks with little or no human involvements [53–56]. Transmission

latency [57–59] refers to the time interval (delay) that occurs when propagating the input data from the source to the destination over a communication link. In rendering enhanced quality of service (QoS) delivery and user quality of experience (QoE), the emerging 5G networks are specified to offer about 10–100 times higher user data rates and lower energy consumptions in comparison to the present LTE based networks [60,61]. These networks will also offer ultra-low and reliable end-to-end latency of less than 1 ms [61] with very high reliability (that is, very low packet error rate). The mMTC paradigm of 5G networks will effectively control and manage the collaboration/interaction of numerous network communication devices by ensuring low device complexities for longer device battery life as a result of low energy consumption.

For efficient transmission of radio signals between mobile devices and base stations, the PHY and MAC layers of 5G cellular networks are designed to consist of numerous building blocks such as spectrum, multiple access technologies, waveforms, frame structures, coding, modulation, beamforming and duplexing techniques as classified in Figure 7 [47]. The waveform candidates for the 5G networks, as shown in Figure 7, include CP-OFDM, UFMC, FBMC, and filtered OFDM (f-OFDM). The classification also include the possible multiple access schemes under considerations for these aforementioned xG networks including: OFDMA, SC-FDMA, resource spread multiple access (RSMA), non-orthogonal multiple access (NOMA) and sparse code multiple access (SCMA) [62–65]. NOMA is a multiple access scheme that uses power domain for the separation of signals that possess remarkable differences in power levels. The SCMA scheme is a non-orthogonal multiple access technique considered for improving the spectral efficiency and transmission latency of xG networks where input coded data streams (at the transmitter) are mapped to codewords of several multidimensional sparse codewords from specific codebooks. RSMA, on the other hand, is also a potential multiple access technique (under consideration for the upcoming 5G networks and beyond) that uses combinations of low-rate channel and scrambling codes with good correlation properties for the separation of different user signals requiring asynchronous and grantless access.

The eMBB service delivery of 5G is designed to offer very high reliability (that is, very low error probability) and high spectral efficiency in digital communication networks. Noise is an unwanted effect that interferes with the transmission of signals as they travel from the transmitter through the communication link to the receiver. The presence of noise in any communication network highly reduces the reliability of the communication system. To guarantee higher reliability of signal transmission and reception over the multipath fading communication channel, accurate error control coding (ECC) is required to enhance precise detection and correction of errors in these communication networks. Low-density parity-check (LDPC) codes, turbo codes and polar codes are considered as the most-promising ECC schemes for higher reliability and spectral efficiency enhancement in the upcoming xG networks [66–71].

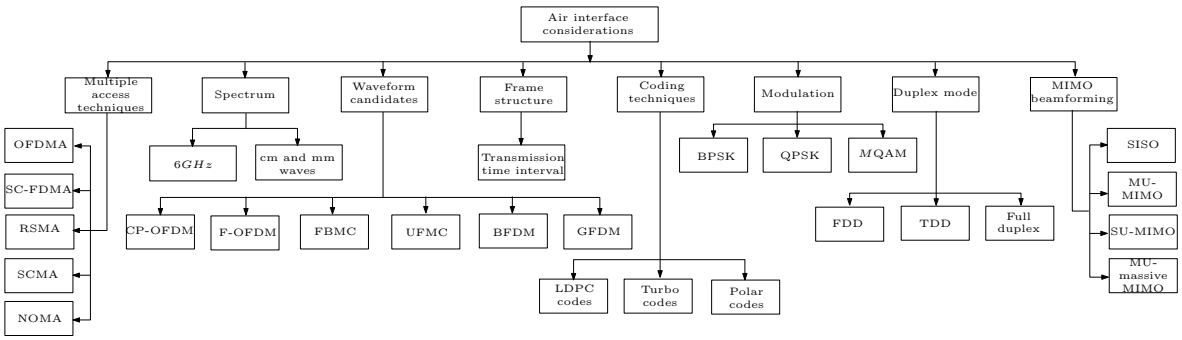

Figure 7. Classification of air interface design considerations for 5G networks.

2.4.2. Candidate Waveforms for 5G Networks

As briefly highlighted in Section 2.3, candidate waveforms under consideration for 5G networks include CP-OFDM, SC-FDMA, f-OFDM, filter bank based OFDM-OAM (FBMC-OQAM), UFMC and

GFDM based transceivers. The features and structures of these waveforms are briefly discussed and compared in this section.

CP-OFDM

One CP-OFDM scheme is a multicarrier modulation scheme [72]. CP-OFDM schemes are deployed for designing well known 3GPP based LTE networks. The digital input data in CP-OFDM systems are mapped using modulation schemes such as *M*-PSK or *M*-QAM in order to form complex symbols which are mapped into orthogonal sub-carriers by frequency to time domain transformation using IFFT. Guard band (or CP) is added to the transmitting symbols in order to give extra robustness to the propagating signals. The inserted CP is used to immune the propagating signals against the unwanted effects of inter-symbol interference (ISI) and inter-carrier interference (ICI) which can arise from multipath propagation as the signals travel over the wireless communication channel to the receiver. The added CP is simply a copy of the tail of the transmitted symbols that is eventually appended to its beginning. The added CP leads to poorer system spectral efficiency due to the added CP overhead. In the emerging 5G networks and beyond, FBMC schemes is considered as a pre-eminent waveform to replace the cyclic prefix-long term evolution (CP-LTE) systems due to the bandwidth wastage incurred from CP insertion as experienced in the design of OFDM systems. The principles of operation and structure of CP-OFDM scheme is well documented in the literature. Readers are referred to [73,74].

SC-FDMA

The SC-FDMA scheme can also be referred to as the DFT-spread OFDM (DFT-S-OFDM) scheme [72,75]. In addition, some text refer to this modulation and multiplexing scheme as linearly pre-coded OFDMA (LP-OFDMA). The structure of SC-FDMA is very similar to CP-OFDM except that an extra pre-coding stage is added in DFT-S-OFDM schemes before the IFFT block. The pre-coding block is used for limiting the PAPR of the transmitted signals. The pre-coding is implemented at the transmitter using an N-point DFT which is applied before the IFFT stage with the aim of mapping the transmitted signals into a number of adjacent-frequency sub-carriers. The reverse process of the above-described procedures is implemented at the receiver where the IDFT is specifically implemented after the FFT block. The structure of DFT-S-OFDM transceivers is depicted in Figure 8. Note that, if the pre-coding block were removed from Figure 8, the set-up could be viewed as a CP-OFDM.

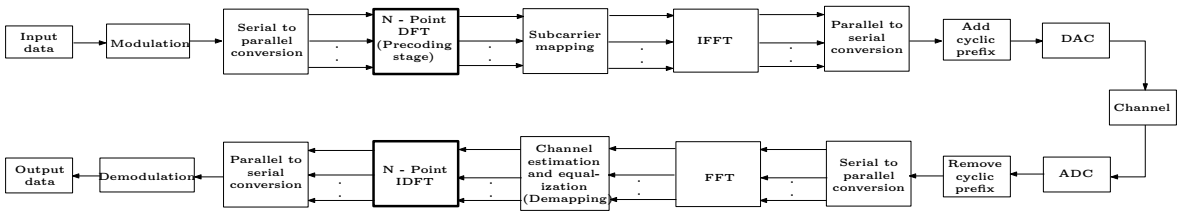

Figure 8. Structure of SC-FDMA modulation scheme.

f-OFDM

The upcoming 5G networks are expected to be allocated a larger bandwidth in order to boost the network data rate [76]. f-OFDM is a recently introduced waveform considered as a potential waveform for the upcoming xG (5G) networks [77,78]. The structure of f-OFDM system is very similar to the conventional CP-OFDM system. The major difference is that, in f-OFDM systems, the assigned system bandwidth is split into subbands. The transmitting baseband signal on each subband is also filtered using a band-limited filter before the transmitting signals travel across the wireless multipath fading channel. The introduced subband based filtering is used for limiting inter-subband interference, which consequently eliminates sidelobe leakages by suppressing OOB emission. In the implementation of f-OFDM transceivers, two broad kinds of filters are considered: soft-truncated

sinc filters and equiripple filters. The impulse response of an ideal low pass sinc filter is an infinitely long sinc function [76], where the long sinc function is adequately soft-truncated using different window functions that may either be Hann window or root-raised-cosine (RRC) window. Equiripple filters are desirable for attenuating inter-subband interference. These filters (equiripple) are designed using Remez exchange algorithm [79] for minimising the maximum error between the desired and actual frequency response [76]. The downlink transceiver structure of f-OFDM is shown in Figure 9. This structure is very similar to the structure of CP-OFDM systems except that subband filtering is introduced, which is not required for CP-OFDM systems. Table 1 shows the differences between f-OFDM and CP-OFDM systems.

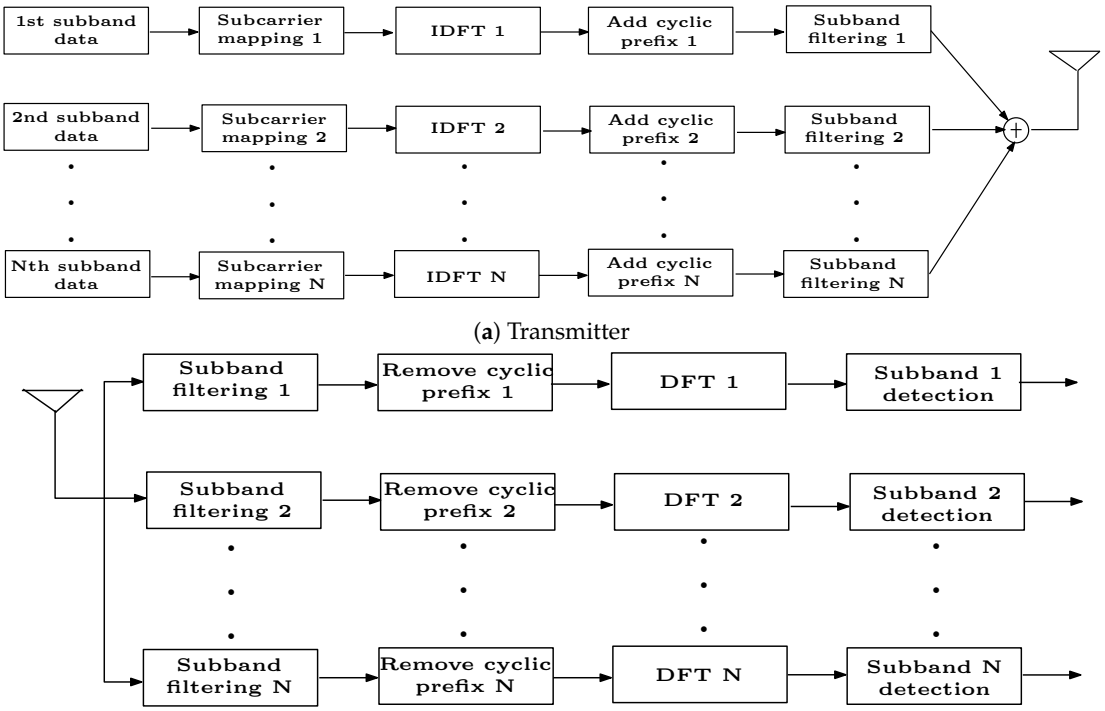

(**a**) Transmitter

(**b**) Receiver

Figure 9. Transceiver structure of f-OFDM.

Table 1. Comparison between CP-OFDM and f-OFDM based systems.

Specifications	CP-OFDM	f-OFDM
Band structure	Single band	Multiple (sub) band
Filtering	Wideband filtering	Subband filtering required
Filter length	Less than length of CP	No longer than half of symbol duration
Sub-carrier spacing	Uniform	Different
Spectral efficiency	Poor	Better (from bandwidth splitting)
Computational Complexity	Low	Higher
Transmission Time Interval (TTI)/Latency	Long	Shorter
OOB leakages	High	Lower (due to subband filtering)
Time domain orthogonality	Orthogonal	Non-orthogonal
Frequency domain orthogonality	Orthogonal	Partly (quasi) Orthogonal
Throughput gain	Low	Higher

Filter Bank OFDM-OQAM

The cyclic prefix block of OFDM systems can be replaced with well-designed filters to form an FBMC system named filter bank OFDM. This waveform can be used with OQAM for the modulation of data symbols and also for maintaining sub-carrier orthogonality within real and imaginary domains. The resulting waveform is known as filter bank OFDM-OQAM (FBMC-OQAM). The use of OQAM and per sub-carrier filtering eliminates the possible need for CP usage in these systems giving rise to

higher spectral efficient systems with improved OOB emission. FBMC-OQAM is well known to suit fragmented spectrum/cognitive radio systems while offering good localisation properties with high robustness against multipath fading. However, the system is inefficient for short burst transmissions as a result of long filter tail [47]. The transceiver structure and principles of operation of this waveform are elaborated in Section 4.1.

UFMC

This is a potential waveform considered for xG networks. UFMC is designed to incorporate the advantages of FBMC systems as well as f-OFDM [80]. This is achieved by grouping the entire band of the OFDM system having N sub-carriers into subbands that are subsequently filtered [47,80]. The complex modulated frequency domain symbols $X(n,k)$ are eventually converted into time domain signals $x(n,k)$ using N-point IDFT conversion as depicted in the synoptic UFMC transmitter structure of Figure 10. The resulting signals are filtered using a bandpass filter $g(n,k)$ to produce the transmitting symbols (with optional CP insertion), which are summed up before been propagated across the wireless multipath fading channel. At the receiver, the transmitted signal is converted in the serial-to-parallel conversion block, filtered and transformed from the time domain to frequency domain, as illustrated in Figure 11. UFMC systems are designed to offer enhanced transmission latency and improved system spectral efficiency similar to FBMC-OQAM systems. These systems (UFMC) are well suited for short bust transmissions [47]. However, the large receiver DFT size of UFMC systems results into very high implementation complexity as compared to other considered waveforms of the emerging xG networks. These systems (UFMC) also suffer from drawbacks such as creation of interference due to partly overlapping subbands.

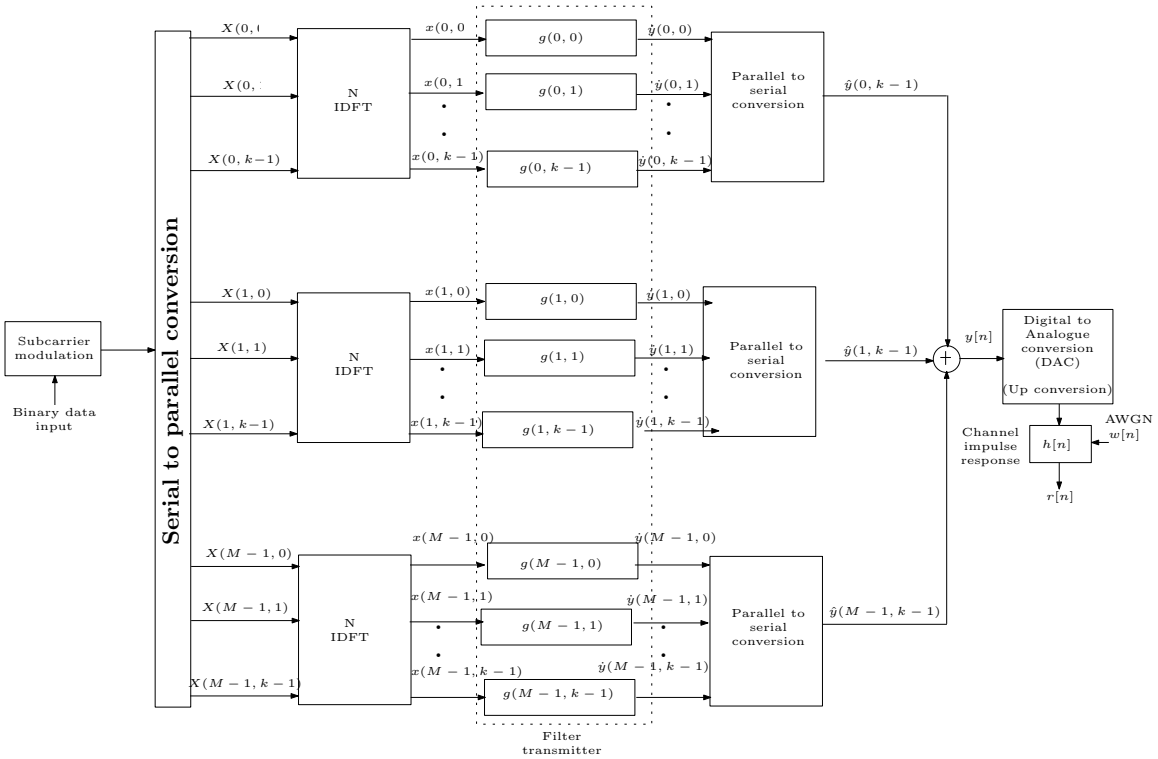

Figure 10. Transmitter structure of UFMC system.

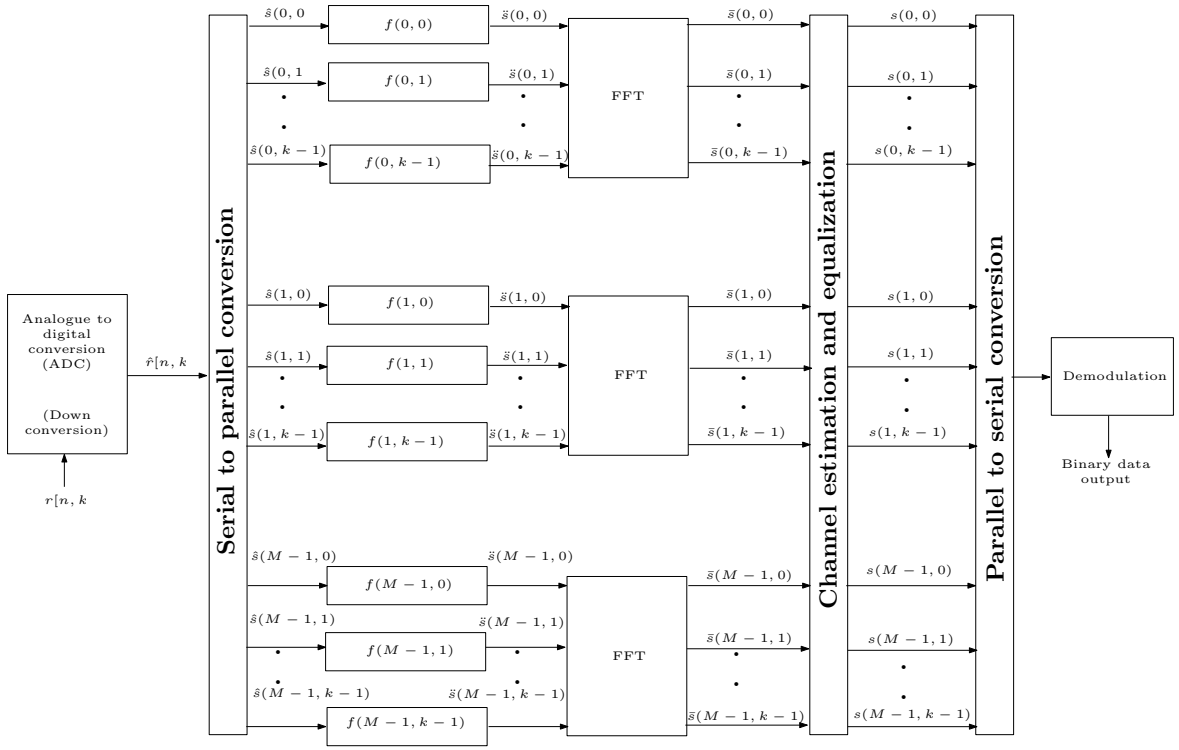

Figure 11. Receiver structure of UFMC system.

GFDM

GFDM is a flexible MCM scheme proposed for the air interface of the emerging next-generation 5G networks [37]. In GFDM schemes, independent blocks are made of a number of sub-carriers and subsymbols, which are modulated independently. Each sub-carrier of GFDM based transceivers is filtered using well-designed frequency and time domain circularly shifted prototype filters in order to curtail the destructive effects of OOB emission. This applied sub-carrier filtering may cause the GFDM sub-carriers to lose orthogonality, which may give rise to ICI or ISI. To keep the system overhead as small as possible, a short cyclic prefix is appended to an entire GFDM block in order to combat possible effects of ISI and ICI. GFDM along with other FBMC waveforms such as filter bank OFDM-OQAM and UFMC are regarded to offer suitable resistance against carrier frequency offsets (CFO). For these reasons, GFDM system is regarded as a block based non-orthogonal MCM scheme [61,81]. Details of the principles of operation and system design of GFDM based transceiver is elaborated in Section 4.2. Table 2 presents a comparison of potential waveform candidates of upcoming 5G Networks.

Table 2. Comparison of waveform candidates of the emerging xG Networks.

Specifications	CP-OFDM	SC-FDMA	f-OFDM	FBMC	UFMC	GFDM
Spectral efficiency	Low	Low	Low	High	High	High
Computational Complexity	Low	Low	Medium	High	High	High
OOB Emission	High	High	Low	Low	Low	Low
PAPR	High	Low	High	Medium	High	Medium
Latency	Medium	Medium	High	High	High	High
Flexibility	High	High	Medium	Medium	Medium	High
Robustness to CFO	Low	Low	Medium	High	High	High

3. Fundamentals of Channel Estimation

As transmitting symbols propagate through the wireless communication channel, they experience several harmful effects from interaction with environmental objects such as buildings, mountains, trees, etc. This results in multipath propagation and signal attenuation. Channel estimation is a useful wireless communication technique that is adopted to ensure accurate detection of the transmitting signals. Over the years, numerous CE techniques have been proposed in the literature to combat the varying nature of the channel. In these proposed CE techniques, the emphasis has been to improve the CE performance, power and bandwidth consumption, and the computational time complexity. As such, we review the CE techniques used in wireless communication applications in general. In particular, we narrow the application of these CE technique to FBMC systems, where we introduce taxonomy to classify these CE techniques.

3.1. Classification of Channel Estimation Schemes

Several CE schemes have been proposed in the literature for estimating the fading channel coefficients in different wireless communication systems. These include the single carrier communication systems such as single-input single-output CP based OFDM (SISO-OFDM), non-contiguous OFDM (NC-OFDM); the multi-carrier communication systems such as multiple input multiple output-OFDM (MIMO-OFDM) systems; and most FBMC schemes such as filter bank OFDM-OQAM and GFDM based schemes. CE schemes can broadly be classified into non-blind (pilot based), semi-blind and blind techniques [82]. In this regard, we classify the CE schemes that have been explored in literature for various wireless communication systems in Figure 12, while explaining the three major class of the CE schemes.

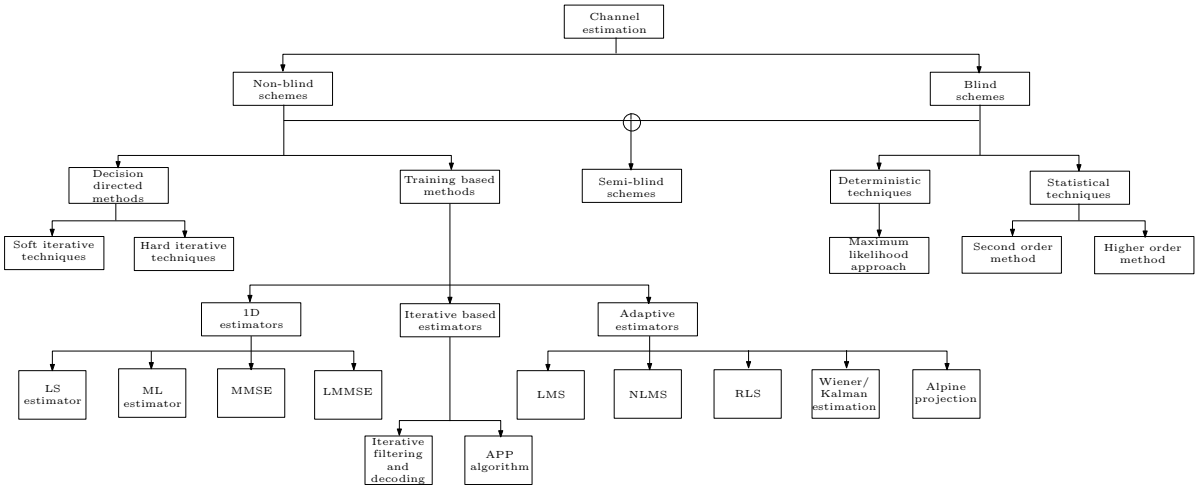

Figure 12. Classification of CE techniques.

3.1.1. Overview of Pilot Based (Non-Blind) CE

Non-blind CE can either be data-aided (training-based) or decision directed CE, as depicted in Figure 12. In training-based CE, also known as pilot-assisted CE, training sequences called pilot symbols, which are known to the receiver, are transmitted along with the data symbols for efficient estimation of the channel [83–85]. If the density of the training symbols used is high, the system CE accuracy improves tremendously; however, the spectral efficiency of the system is decreased due to the introduction of overhead by the pilot symbols [83]. Several works have been reported in the literature to address the challenges of pilot-assisted CE schemes for various telecommunication techniques such as SISO-OFDM, NC-OFDM and MIMO-OFDM schemes. In [86], the performances of two time domain CE techniques named least square (LS) and minimum mean square error (MMSE) CE schemes are investigated for OFDM systems in a slow fading multipath channel. The basic LS and MMSE channel

estimates as reported in [86] are modified and estimated through multipath fading channel assuming different number of taps. It is observed from results obtained in [86] that the MMSE CE scheme demonstrates superior performances over LS in terms of mean square error (MSE) and symbol error rate (SER) at various levels of signal-to-noise ratio (SNR). In [73], the performances of three CE schemes (LS, linear MMSE (LMMSE) and least mean square (LMS)) are investigated for SISO-OFDM based transceivers under two channel types: auto-regressive based fading channel and multi-path Rayleigh fading channel. In addition, [73] assumed different kinds of pilot arrangements while adopting *M*-ary quadrature amplitude modulation (*M*-QAM), where *M*=16, quadrature phase shift keying (QPSK), binary phase shift keying (BPSK) and differential QPSK (DQPSK) as the underlying modulation schemes. In [87], the challenges of pilot-aided CE in OFDM systems are addressed using time domain channel statistics on an additive white Gaussian noise (AWGN) channel. Channel estimation schemes such as LS, MMSE and DFT based CE were deployed in [87]. In addition, in [87], the autocorrelation matrix of the channel and the noise variance are obtained using noise suppressed channel impulse response where results are analysed in terms of MSE and SER. From the results obtained, the MMSE estimation scheme demonstrates the best performance in comparison to the LS and DFT based CE schemes, and the LS offered the worst performance. A comparison of two pilot-aided CE techniques is analysed in [88] for OFDM systems, where the performances of maximum likelihood estimator (MLS) and Bayesian MMSE estimator (BMMSEE) are investigated. The MLE does not require information of the SNR and channel statistics while the BMMSEE exploits prior information about the channel. This makes the MLE simpler to implement but the BMMSEE demonstrated a better accuracy at low SNR. However, it is concluded that, at higher and intermediate SNR, the performances of both schemes are comparable. The CP that is inserted into the conventional OFDM system offers enhanced robustness for combating the undesirable effects of multipath fading. OQAM is adopted in digital communication systems for maintaining the orthogonality of sub-carriers as they transmit their signals over the wireless fading channels. The inclusion of CP to OFDM systems using OQAM modulation (that is, CP-OQAM-OFDM) can be used to ensure quality signal reception at the receiver end. In [89], the performances of two estimators named weighted least squares (WLS) and pairs of pilots (PoP) are analysed for CP-OQAM-OFDM system, where corresponding Cramér–Rao bounds (CRB) are used for comparison. The proposed PoP channel estimator in [89] offers lower computational complexity at the receiver as compared to the transmitter. This estimator offered good and similar bit error rate (BER) CE performance in comparison with WLS estimator.

In decision directed CE (DDCE), training symbols are adopted for CE as well as the re-modulated detected message symbols [85,90,91]. In these CE schemes, CE of previous symbols is used for data detection of the current estimates after which the newly detected data are used for estimating the current channel. The detection of data in DDCE can be achieved either by hard or soft decision where bitwise detection is adopted for soft decision and a specific constellation is forced for hard decision [92]. An MSE expression for DFT based DDCE schemes in *M*-ary phase shift keying (MPSK) for LTE-A downlink transmission system is proposed in [93]. Simulation results from this scheme are compared with practical systems based on long term evolution-advanced (LTE-A) downlink standards. Moreover, in [94], a novel soft DDCE technique is proposed that estimates the channel of interfering signals based on demodulation reference signal (DM-RS) using virtual pilot signals (VPS) for multiuser MIMO-OFDM (MU MIMO-OFDM) based transmission scheme. In this algorithm, reliable data tones are chosen from the desired and interfering signals as VPS, after which the quality of CE is improved by using iterative detection and decoding (IDD) scheme. The proposed algorithm shows superior performance gain over the conventional approaches that adopt either single user detection (SUD) or multiuser detection (MUD) such as the conventional MMSE for both SUD and MUD. It is worth mentioning that several pilot-based (or non-blind) CE techniques with captivating results (apart from the above mentioned) have been set down in writing for SISO cyclic prefix based OFDM systems. Some of these techniques are compared and summarised in Table 3.

Table 3. Summary of CE techniques for non-filtered multicarrier modulation schemes.

Reference	Aim of Research	CE Schemes Applied	Applicable Technique or Waveform	Approach	Obtained Results
[86]	Time domain channel statistics pilot based CE over AWGN	LS and MMSE	Pilot-based CE for SISO-CP-OFDM	CE modifications assuming finite length impulse response	MMSE CE demonstrated superior performance over LS CE in terms of MSE and BER
[87]	Time domain channel statistics pilot based CE over AWGN	LS, MMSE and DFT based CE	Pilot-based CE for SISO-CP-OFDM	Time domain estimation of noise variance and channel autocorrelation estimation using denoise CIR	The MMSE estimator demonstrated superior performance to DFT based CE with LS offering the worst CE performance
[88]	Performance investigation of MLE and Bayesian MMSEE estimators over multipath fading channel	MLE and Bayesian MMSEE	Pilot-aided CE for SISO-CP-OFDM	Bayesian MMSEE Exploitation of prior channel information	• CE at bandwidth edges are worse than CE in the middle • Bayesian MMSEE performs better than MLE at low SNR • Bayesian MMSEE and MLE have comparable performances as SNR increase
[89]	To design optimal CE schemes for CP-OQAM-OFDM system in comparison to OQAM-OFDM system	WLS and PoP estimators	Pilot-aided CE for SISO-CP-OQAM-OFDM	• Insertion of zero symbols for interference avoidance and minimisation of weighted least square error for WLS estimator • Transmitter pilot design determined by real data symbols	• PoP offered similar BER performance for CP-OQAM-OFDM with low computational complexity as compared to WLS • The estimators offer better robustness to multipath delay spread for CP-OQAM-OFDM especially in broadband systems in comparison to OQAM-OFDM systems
[93]	Development of an analytic MSE formula for DDCE schemes in *M*-ary PSK modulated OFDM	Two dimensional DFT based DDCE	Pilot-based CE for SISO-CP-OFDM based on LTE/LTE-A	Dependent and identically distributed coded bit error	Simulated MSE performance obtained using the developed formula matches practical values for downlink LTE-A systems

Table 3. *Cont.*

Reference	Aim of Research	CE Schemes Applied	Applicable Technique or Waveform	Approach	Obtained Results
[94]	Design of a novel CE technique for MU-MIMO OFDM systems	Virtual pilot based CE using iterative detection and decoding (IDD)	Pilot-assisted DDCE for MIMO -OFDM	• Estimation of channel information of interfering signals using demodulation reference signal (DM-RS) • CE improvement using reliable data tones form desired and interfering signals	Proposed estimator achieves substantial block error rate (BLER) performance gain over conventional single user CE schemes such as MMSE with SUD and MUD
[95]	Development of an inverse channel based blind CE (ICBCE) scheme for CP-OFDM to improve the CE performance with limited number of received blocks	ICBCE for CP-OFDM	Blind CE for SISO-CP-OFDM	• Development of a predetermined null subspace that corresponds to the transmitted CP-OFDM signal vector subspace • Exploitation of the inverse CIR vector orthogonality property to predetermined null subspace	• ICBCE scheme outperforms the existing re-modulation based blind CE (RMBCE) and repetition based blind CE (RPBCE) techniques in terms of MSE at low numbers of received blocks and SNR values • ICBCE offered lowest implementation complexity
[96]	Design of a novel semi-blind iterative space alternating generalised expectation (SAGE) based CE for massive MIMO systems	Semi-blind iterative SAGE CE	Pilot/data-assisted SAGE based CE for Massive MIMO	Iterative update of pilot based MMSE using SAGE algorithm	• The proposed SAGE based estimator converges in almost a single iteration • Proposed estimator offers improved BER/MSE performance over existing pilot and data-aided channel estimators in pilot contaminated scenarios

Table 3. *Cont.*

Reference	Aim of Research	CE Schemes Applied	Applicable Technique or Waveform	Approach	Obtained Results
[97]	Design of blind ML detection with single orthogonal space time block codes OFDM (OSTBC-OFDM) blocks	Semi-blind/blind CE based on use of minimal training sequence	Semi-blind/blind CE for OSTBC-OFDM	• Grouping of subchannels for reduction complexity detection schemes using low complexity cyclic ML scheme • Use of limited pilots for ensuring a probability one identifiability condition in semi-blind estimation	• The proposed scheme outperforms pilot-based LS and differential technique in terms SER • The proposed scheme achieves lower computational complexity in comparison to non-blind counterparts
[98]	Design of a low complexity semi-blind CE technique and recording scheme for two-way relay networks	Semi-blind CE based on MSE	Second order statistics based semi-blind CE for two-way relay networks	• Pre-coding based on rotation based matrix and composite CIR of source-relay-destination links based on second order statistics of received signals • Using small training blocks • MSE evaluation of CE for infinite number of data blocks and high SNR regime	• The NMSE of the estimates is inversely proportional to the SNR • The NMSE of the estimates is also inversely proportional to the data block
[99]	Derivation of a quasi-Newton based procedure for semi-blind CE in uplink cloud radio access networks (C-RANs)	Semi-blind CE based on quasi-Newton method	data symbols CE method	• Implementation of initial CSI • Brayben, Fletcher, Goldfarb and Shanno (BFGS) algorithm using data and pilot symbols for estimating CSI using ML principle	• The proposed scheme offers significant MSE improvement by the utilisation of data symbols over conventional LS CE • The spectral efficiency of the system is improved because data symbols are utilised instead of increasing number of pilot symbols that can create an overhead

In recent times, NC-OFDM has been proposed for higher data rates transmission in cognitive radio context [100,101]. This NC-OFDM technique employs the use of continuous/contiguous blocks of sub-carriers for the transmission of data symbols. In these systems, the sub-carriers been utilised by the PUs are deactivated by the secondary users (SUs) with the sole aim of avoiding license users (LUs) interference [102,103]. Channel estimation is not well studied for NC-OFDM [103]; however, some CE algorithms have been proposed and implemented in the literature by many researchers to improve the performance of the NC-OFDM system. According to [104], it has been proven that equispaced and equipowered pilot tones yields the optimal pilot design for conventional OFDM but this does not hold true for an NC-OFDM system. A new pilot symbol design for CE in NC-OFDM based cognitive radio systems is proposed in [105]. In this proposed method, convex optimisation and cross entropy optimisation are adopted for designing of pilot symbols with the purpose of minimising the MSE of the channel estimate for frequency selective fading channels. In [100], a new LS CE algorithm is proposed for NC-OFDM systems in cognitive radio context. In this proposed scheme, LS CE is adopted and modified for obtaining the channel fading coefficient of sub-carriers that transmits the pilot symbols. Least square CE with IDFT based noise reduction is proposed to improve CE accuracy while pilot-block average based noised reduction (PBANR) is proposed to further improve the performance of CE for slow time-varying channels. Simulation results show that these proposed algorithms offer better performance than the conventional LS CE method. An improved time domain CE method based on the principles of spectrum sensing adopted at transmitter and receiver is proposed in [101] in order to improve the performance and reduce noise for NC-OFDM systems. This proposed method outperforms the DFT based and the conventional LS CE methods.

On the other hand, the greedy algorithms include matching pursuit (MP), orthogonal matching pursuit (OMP), stagewise orthogonal matching pursuit (StOMP), regularised orthogonal matching pursuit (ROMP), and compressive sampling matching pursuit (CoSaMP). Active research is carried out in the field of CS which finds many applications in mathematics and signal processing communities [106]. The application of CS techniques to sparse CE employs fewer pilot symbols to estimate the channel. Two main classes of algorithms are considered for CE based on CS in [107]: convex optimisers (linear programming) and greedy algorithms. The linear programming method is based on basic pursuit (BP) and gradient projection for sparse reconstruction (GPRSR), subspace pursuit (SP), and sparsity adaptive matching pursuit (SAMP) algorithms. For NC-OFDM systems, sparse CE techniques have been implemented using OMP and SAMP algorithms. In [108], CE based on CS is investigated where the subspace pursuit algorithm is deployed. The authors of [107] investigated CS based CE, where OMP, SAMP and modified adaptive matching pursuit (MAMP) algorithms are adopted to estimate the channel for NC-OFDM based transceivers. Results were obtained in terms of the MSE, where the MAMP, SAMP, and OMP show superior performance in descending order as compared to the LS method.

Channel estimation is proposed for SC-FDMA communication systems in [109–111]. Three novel CE methods are proposed in [109] for estimating the channel fading coefficients of LTE based SC-FDMA systems over time-varying multipath channels. The estimators are named frequency domain LS (FDLS), frequency domain LMMSE (FDLMMSE) and FDLS estimator with constant windowing (FDLS/CWD). The proposed FDLS CE in this research work [109] is different from the conventional LS technique as it consists of three components that include: the FD real CIR on individual sub-carriers over a symbol duration, the inter-channel interference term and the noise term. The proposed FDLMMSE estimator takes into account the channel auto-covariance matrix, the initial FDLS CIR, as well as the transfer domain AWGN power. One significant feature which distinguishes the proposed FDLMMSE estimator from the conventional LMMSE scheme is the assumption that the receiver at any instance of time has an on-time correlation matrix. To enhance the CE performance in noise-dominant environment, the FDLS/CWD channel estimate is proposed by exploiting the correlation of the channel transfer function (CTF). In the CWD approach, a regular sliding window is adopted for smoothening the obtained FDLS channel estimates on sub-carriers. Results obtained demonstrate that the FDLMMSE estimator

offers the best performance in terms of MSE, and the FDLS estimator offers the worst performance at low SNR values. The FDLS/CWD shows similar BER performance to FDLMMSE at low SNRs while exhibiting degradation in performance at high SNR values due to the effects of self-interference. Hence, the FDLMMSE channel estimator offers the best performance in both low and high SNR ranges. In [110], an improved CE based on DFT-LS is proposed in comparison to conventional LS and traditional DFT-LS methods. In the proposed improved DFT-LS estimator, conventional LS estimated values are improved upon by time-domain extraction of the CIR length through in and out estimation of the CP which is set to a particular threshold in order to eliminate the system generated noise. The proposed improved DFT-LS CE algorithms demonstrated superior BER performances in low SNR values. At higher SNR values, the proposed estimator performances deteriorate rapidly in proportion to the selection of the threshold value that is employed for the elimination of noise. The performances of channel estimators such as LS, FIR, Gauss–Markov (GM), LMMSE and NLMS are analysed in [111] for SC-FDMA systems at three different user speeds of 3 km/h, 50 km/h and 120 km/h. Results obtained in terms of SER demonstrate that all compared CE schemes exhibit similar performances, although the LMMSE estimation scheme offers the best CE performance for SC-FDMA multiplexing schemes at low SNR ranges under very low user speed (3 km/h) conditions. The GM algorithm offers the best CE performance at high SNR values under same conditions. Similarly, at medium user speed (50 km/h), the LMMSE estimator offers the best CE performance at low SNR ranges while GFDM estimator performs best under high SNR conditions. In both low and high SNR conditions, LMMSE CE demonstrates the best performance as compared to all the estimators under very high speed conditions (120 km/h).

BFDM is a waveform under potential consideration for next-generation networks which employs well-localised pulse shapes at both transmitter and receiver [37]. The applied transmitter and receiver localised pulse shapes are designed to be bi-orthogonal to each other where the high quality frequency localisation of transmit pulses offer extra robustness against Doppler effects (frequency dispersion). The good time localisation of the pulses gives extra robustness to this multicarrier system against the effects of multipath fading (time dispersion) using OQAM technique. CE for BFDM-OQAM transceivers is still an open research area. In fact, to the best of our knowledge, the only research work documented to analyse the performance of CE schemes for BFDM-OQAM is in [112]. In [112], a low complexity ML based channel estimator is proposed for BFDM-OQAM systems in dispersive time-varying channels which uses the correlation matrix of channel parameters for CE. The performance analysis of the proposed ML-based CE as reported in [112] demonstrates that the estimator offers appreciable robustness against frequency dispersion of channels. UFMC is a novel waveform that combines the simplicity features of CP-OFDM systems in addition to the robustness of FBMC systems. Due to the familiarity of these systems (UFMC) with conventional OFDM systems, UFMC is also known as universal filtered OFDM (UF-OFDM) [113]. CE is also not well researched for UFMC systems in the literature. The authors of [113] studied and analysed the performance of CE in UFMC based systems. In this study, the procedure and performance of pilot-aided CE are investigated for UFMC systems where it is revealed that training based CE and pilot structure is applicable to UFMC systems by pre-compensation of the FIR filter at the transmitter. In the investigated CE method, raw channel estimates are obtained at pilot locations using LS and LMMSE schemes where the obtained estimates are subsequently improved using the sliding window (SW) approach. In the SW approach, the variance of the noise signal is significantly reduced in proportion to the SW size. The performances of the investigated CE schemes are analysed using three kinds of communication channels which include AWGN channel, frequency-flat fading channel (with user travelling at 50 km/h) and frequency-selective fading vehicular-A channel. Simulation results obtained show that the UFMC system achieves the same or slightly better SER performance in comparison to LTE based CP-OFDM systems under all considered channel conditions using SW algorithm.

3.1.2. Overview of Semi-Blind Channel Estimation

In semi-blind CE, signal's statistical properties as well as training sequences are incorporated to estimate the CIR of the channel. This means that semi-blind methods are hybridisation of the pilot based techniques and blind methods. In [96], semi-blind iterative SAGE maximisation CE algorithm is proposed for massive MIMO systems that makes use of data symbols for CE. In this system, the base station is assumed to have knowledge of its own cell's large scale fading coefficients without being aware of interfering cells. This novel CE algorithm is designed to update the training-based MMSE CE iteratively using SAGE algorithm where the initial estimate is improved by employing pilot symbols and soft information of the transmitted data. This proposed algorithm demonstrates superior performance in comparison with other semi-blind and blind CE schemes reported in the literature. In [98], a low complexity pre-coding and semi-blind CE scheme is proposed for a two-way multi-relay networks under frequency selective fading channels. The proposed method makes use of a rotation based matrix for pre-coding, and the composite CIR of each source relay-destination link is estimated using second-order statistics of the received signals. A small number of pilot symbols is adopted to eliminate the ambiguity in the proposed CE which is caused by the channel information of the direct link. The results obtained in [98] shows that the MSE of the channel estimate varies inversely to the number of training blocks and the SNR as the number of data blocks approaches infinity. It is worth mentioning that a quasi-Newton method for semi-blind CE named BFGS estimation scheme is proposed in [99] for uplink C-RANs. The CE scheme utilises unknown data symbols and known training sequence to estimate the channel distortion. Furthermore, Ban, Y. [99] adopted the maximum likelihood (ML) principle to improve the performance of the CE. Results show that their algorithm decreases the overhead of bandwidth without sacrificing the MSE performance. Besides, the semi-blind algorithm demonstrates high data throughput and spectral efficiency for C-RAN as compared to the pilot aided CE scheme investigated in [99].

3.1.3. Overview of Blind Channel Estimation

The blind CE scheme requires many data and it is known for exploiting the statistical and mathematical properties of the transmitted data [92]. As shown in Figure 12, the blind CE techniques in the literature fall under two class: deterministic and statistical blind CE. Deterministic CE schemes offer better performance in comparison to statistical CE schemes at the expense of very high computational complexities which further increases with increase in the modulation constellation order. Blind CE schemes are known to be bandwidth efficient since they do not require training symbols in order to estimate the channel. However, they usually exhibit very high computational complexity.

Several works in the literature adopt the blind CE techniques for different wireless communication technologies. A subspace based blind CE (SBCE) algorithm that is not affected by null subspace CE errors caused by noise and fading algorithm is proposed for CP-OFDM (ICBCE) schemes in [95]. The performance of this algorithm is compared with two conventional SBCE CE algorithms: RPBCE scheme and RMBCE scheme. It is known from the literature that the RPBCE scheme exhibits very high computational complexity. As such, the RMBCE scheme is designed to offer lower computational complexity in comparison to RPBCE schemes. Nevertheless, the performances of both schemes are similar. The ICBCE algorithm outperforms both conventional SBCE schemes (that is, RMBCE and RPBCE) in terms of MSE at low SNR values and it also offers lower computational complexity. Several OSTBC based MIMO-OFDM schemes have been reported in the literature and are designed to exploit the OSTBC structure together with the inter-sub-carrier relationships caused by the FIR channel model. These CE schemes are known for their very high computational complexities. Some works (such as the sub-channel grouping technique) have proposed different methods capable of reducing the computational complexities of existing OSTBC CE schemes.

Most blind CE algorithms are usually applicable to a single block of OSTBC-OFDM data [97] and are only efficient in flat fading channels especially in MIMO-OFDM schemes. In [114], a blind CE scheme is proposed for OSTBC-OFDM schemes that take advantage of the structural properties

of OSTBCs, where the processing across all sub-carriers are done coherently. This proposed scheme is efficient in time-varying channels and has no limitations on the number of transmit and receive antennas in comparison to other schemes. The algorithm proposed in [114] exploits a semi-definite relaxation (SDR) technique for converting the blind CE problem to a convex semi-definite programming (SDP) form. Substantial simulation performance is demonstrated in comparison with several conventional blind MIMO-OFDM based CE schemes in the paper [114]. It was mentioned in Section 2.4.2, that the addition of CP to CP-OFDM based transceivers for the purpose of combatting ISI and ICI, as well as the appending of training symbols for the purpose of CE results into significant degradation in system spectral efficiency. The performance of isotropic orthogonal transform (IOTA) based multicarrier transceiver is proposed as an alternative to CP-OFDM systems. This technique employs the use of well-designed pulse shaping with good frequency and time localisation properties for limiting system interference, as well as sustaining sub-carrier orthogonality in real field without the use of CP.

3.2. Channel Estimation for Filter Bank OFDM-OQAM

CE is currently an active research area for FBMC-OQAM based transceivers [115–117], while different CE schemes have also been proposed in the literature for filter bank OFDM-OQAM systems. The CE schemes for filter bank OFDM-OQAM can be broadly classified as preamble based or scattered plot based CE. Accordingly, we classify the CE techniques adopted in the literature for filter bank OFDM-OQAM in Figure 13. Besides, we present a review of the CE techniques shown in Figure 13.

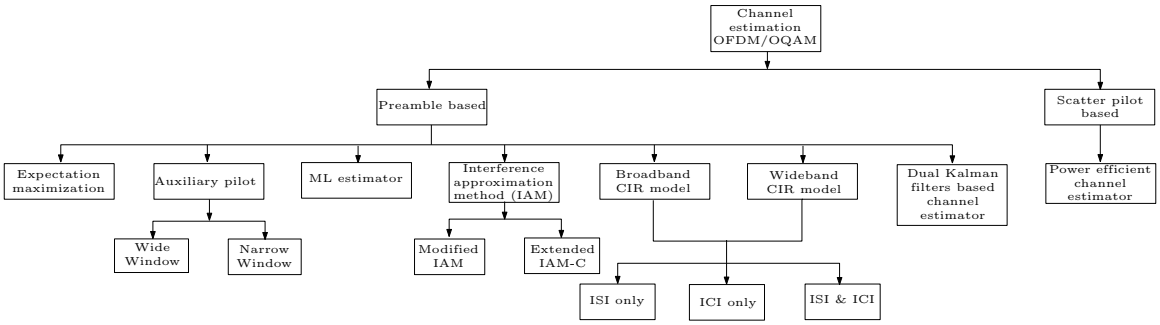

Figure 13. CE schemes for filter bank OFDM-OQAM.

In [118], pilot aided channel estimation schemes are implemented for estimating channel coefficients in OFDM-OQAM based communication system. A new preamble aided estimation scheme named modified interference approximation method (MIAM) is developed from the original interference approximation method (IAM) scheme for estimating channel conditions. The results are compared with existing methods such as the wide and narrow auxiliary pilot (AP) schemes. The proposed scheme (MIAM) is designed to solve the suffering of pilot symbol imaginary interference. However, from the results obtained, AP scheme achieves better estimation performance in terms of mean square error and bit error rate. In [119], a preamble-based CE scheme is proposed to improve the existing IAM estimation method. The IAM CE technique depends on the knowledge of pilot neighbourhood for the approximation of interference in order to improve CE performance. This technique (IAM) consists of IAM-R and IAM-C where R and C are real and imaginary pilot symbols, respectively. In the IAM-C method, the pilot symbols are imaginary (complex) where offset quadrature phase shift keying (OQPSK) is assumed. The proposed algorithm in [119] extends the IAM pilot-based algorithms (which have nulls at neighbouring time instants) and is built into a structure that consists of significantly larger pseudo-pilots. This new structure is called extended IAM-C (E-IAM-C). From this work, the proposed E-IAM-C algorithm provided a better estimation performance when compared to IAM-R and IAM-C. In [120], a short preamble-based CE algorithm is developed where the preamble consists of only one pilot FBMC symbol for highly frequency selective

channels in OFDM-OQAM systems. Simulation results demonstrate the effectiveness of this algorithm in both frequency and time domain IAM-C CE methods for mildly and highly frequency selective channels. A novel pilot design scheme named composite pilot pair (CPP) which takes advantage of the filter's localisation properties for a simple CE method at receiver is proposed in [121]. It captures the major part of channel induced distortions. The results are compared with existing AP schemes in terms of mean square error (MSE) and un-coded BER. The proposed CCP demonstrates superior performance in comparison to the existing AP schemes. In [122], a novel preamble-based algorithm is proposed for narrowband per-subcarrier maximum likelihood (ML) CE. This new method is based on the ML channel estimator. The major extension in this method involves the assumption that only the training sequence transmitted in the observed sub-carrier is known while unknown (data) symbols are transmitted in two neighbouring sub-carriers that are immediately adjacent to themselves. This new CE method is improved using the expectation maximisation (EM) algorithm and it is designed to iteratively approach and improve the ML estimator's performance. The EM-ML channel estimator is known for providing an increase in spectral efficiency as only a few numbers of sub-carriers are filled with training symbols. In [115], a performance comparison between two models for the received sub-carrier signals is made. This includes a per-subcarrier broadband channel model as well as its narrowband equivalent. Three cases of interference embedded CE schemes are considered and applied to both the broadband and narrowband channel models. These interference embedded CE techniques involve CE in the presence of ISI only, ICI only and in situations of both ICI and ISI. From the results obtained, both broadband- and narrowband-based models offer the best normalised mean square error (NMSE) performances when only ISI is considered. ICI comes next in estimation performance while estimation in the presence of both ICI and ISI offers the worst CE performance. Estimation of time-varying channels is adopted in [123] where dual optimal Kalman filters are introduced for estimating fading channel statistics as well as their unknown pth order autoregressive parameters in an OFDM-OQAM based wireless system. This proposed method estimates the fading coefficients at pilot symbol positions while linear, spline and low-pass interpolation are adopted for estimating data position fading coefficients.

3.3. Channel Estimation for Filter Bank GFDM

Channel estimation for filter bank GFDM is a new research area waiting to be exploited, especially in filter bank GFDM-OQAM. Very little research has been carried out in this area in terms of developing algorithms for estimating the channel fading. In fact, to the best of the authors' knowledge, no CE algorithm has been proposed in the literature for filter bank GFDM-OQAM. As such, more work can be done in this research area in order to effectively estimate the channel distortion, in particular, adopting the semi-blind and blind based CE techniques. Nevertheless, we classify the techniques adopted to estimate the channel distortion in filter bank GFDM in Figure 14. The classification is based on the general knowledge of CE techniques. Moreover, we summarise some of the CE technique adopted in filter bank GFDM in Table 4.

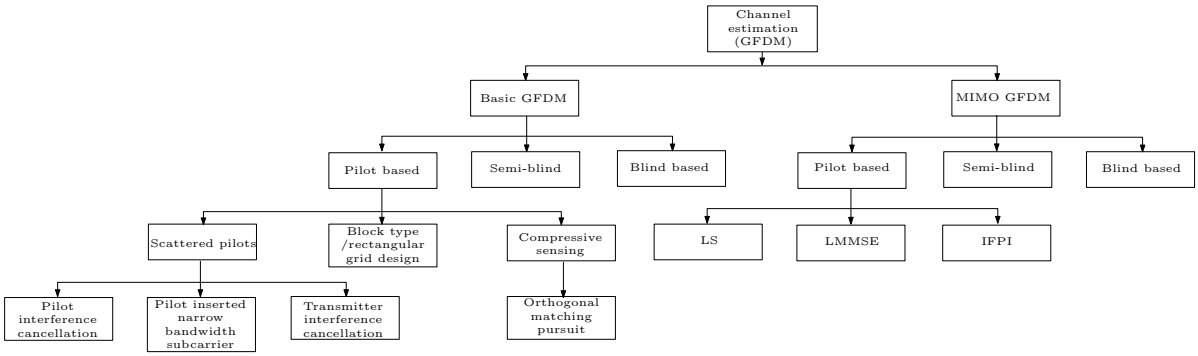

Figure 14. CE schemes for conventional GFDM.

Table 4. Summary of CE techniques for filter bank multicarrier modulation schemes.

Reference	Aim of Research	CE Schemes Applied	Applicable Technique or Waveform	Approach	Obtained Results
[51]	Modification of GFDM systems for CE using orthogonal pilot insertion method for interference free CE	Interference free pilot insertion (IFPI) based CE	Pilot-assisted CE for GFDM transceivers	Insertion of pilot subsymbols such that received symbol frequency domain at pilot frequencies have no influence from the data subsymbols for IFPI CE	• IFPI GFDM has slightly higher OOB emission as compared with the conventional GFDM. • The MSE of the proposed IFPI technique is identical to the conventional OFDM • The PAPR of proposed IFPI GFDM is higher than the basic GFDM
[112]	Reduced complexity CE for BFDM-OQAM transceivers in dispersive time-varying channels	Training-based CE for BFDM-OQAM	ML based CE for BFDM-OQAM based transceivers	ML CE based on use of correlation matrix	Proposed estimator offers significant robustness against Doppler spread
[113]	CE for UFMC based transceivers using FIR pre-compensation and SW approach	Pilot-aided CE for UFMC based transceivers	LS and LMMSE based approach for UFMC systems	• Training-based CE by FIR filter pre-compensation at transmitter • Reforming of obtained raw channel estimate using SW approach	UFMC achieves the same or slightly better SER performance under AWGN and frequency/flat fading vehicular-A channels in comparison to CP-OFDM systems using SW approach
[115]	Development of a novel narrowband per-subcarrier ML CE scheme for FBMC systems	EM based CE	Preamble-based CE for FBMC based transceivers	• EM-ML CE under the assumption that only pilot symbols transmitted in observer sub-carrier is known while unknown data symbols using the two immediate adjacent sub-carriers • The CE method is based on the EM algorithm,, which allows the performance to converge iteratively to the ML solution	The EM-ML estimator offers improvement in spectral efficiency using few sub-carriers that are filled with training symbols

Table 4. *Cont.*

Reference	Aim of Research	CE Schemes Applied	Applicable Technique or Waveform	Approach	Obtained Results
[119]	Performance analysis of Extended-IAM preamble-based CE scheme in comparison to IAM scheme	E-IAM preamble based CE	Preamble-based CE for Filter bank OFDM-OQAM	Design of a preamble structure which exploits the symmetry of the interference weights for generating pseudo-pilots of higher magnitude than IAM-C	The E-IAM-C algorithm demonstrates superiority over IAM-R and IAM-C techniques in terms of NMSE at various SNR values over mildly and highly frequency selective fading channels
[118]	Development of two novel CE schemes for filter bank OFDM-OQAM based transceivers	Pair of real Pilots (PoP) and IAM preamble based CE	Pilot-based CE for OFDM-OQAM	• Design of CE without requiring the *a priori* knowledge of the orthogonal prototype function (PoP). • Design of CE using knowledge of the orthogonal prototype function with approximation of the interference term at the receiver side (IAM)	OQAM-IAM method demonstrated superior performance in comparison to OQAM-PoP in both CP-OFDM and OFDM-OQAM based transceivers
[122]	Performance comparison of three variants of interference embedded CE	• CE in the presence of ISI only • CE in the presence of ICI only • CE in the presence of both ISI and ICI	Preamble-based CE for FBMC-OQAM based transceivers	• Estimation using broadband-based channel model • Estimation using narrowband-based channel model	• Both broadband and narrowband models offered good CE performance in terms of NMSE in the presence of ISI only • Both broadband models offered poor performance in presence of both ICI and ISI
[124]	Design of training sequence for IQ imbalance and CE in GFDM systems with low complexity receiver	Training sequence design for IQ imbalance estimation	Preamble-based CE for GFDM transceivers	Sparse frequency domain based training sequence design over low complexity GFDM systems	The proposed technique improves the BER performance of GFDM systems in comparison to uncompensated case
[125]	• Design of a novel iterative CE scheme based on OMP CS technology for GFDM transceivers • Derivation of CRB for CE in GFDM transceivers	CS based OMP CE	Pilot-based CE for GFDM transceivers	Adoption of OMP technology for accurate CE to yield precise reconstruction of ICI	• Simulation results confirmed the efficient performance of the proposed CS based OMP CE scheme over severe interference cases • Performance of proposed estimator is equivalent to CRB methods

In [126], two novel pilot based CE methods (pilot interference cancellation (Pilot-IC) and transmitter interference cancellation (Tx-IC) are proposed for estimating the fading channel coefficients for GFDM based transceivers with QAM modulation (GFDM-QAM). In Pilot-IC, interference is only pre-cancelled at pilot symbols while interference is simultaneously pre-cancelled at both pilot and data symbols for Tx-IC. These estimation algorithms are realised with scattered pilots over time and frequency grid, thereby ensuring a reduction in overhead. Thus, this makes it possible to estimate the channel fading over frequency selective and time-varying channels. The performances of the two proposed CE schemes are analysed in terms of MSE and un-coded BER for time-invariant frequency selective pedestrian B (PB) channels, where pilot symbols are scattered over the sub-carriers of one GFDM symbol with interpolation performed in the frequency domain.

Moreover, in [126], the CE performances of the two proposed algorithms are compared with the CE performance of conventional OFDM. The initial results obtained show that the two proposed algorithms demonstrate the same MSE performance and comparable performance with OFDM. The performances of both CE techniques are analysed for matched filtering (MF) and zero forcing (ZF) receivers using the same PB channel. It is observed from the un-coded BER performances that both pilot-IC and Tx-IC have the same BER performance, which is also comparable to OFDM systems. The BER performance of the two proposed CE algorithms for GFDM system is analysed for various transceiver settings over AWGN channel. It is observed that GFDM systems using Tx-IC transmitter as well as MF receiver with Tx-IC CE offers relatively the same performance as GFDM system with Pilot-IC transmitter and zero forcing receivers with Pilot-IC CE. Since the two proposed CE schemes demonstrate similar performances, it is concluded in [126] that interference can be cancelled at either the transmitter or the receiver.

In [125], the proposed CE scheme in [126] is compared with a novel CE scheme that is based on CS technology by the exploitation of approximate sparsity of CIR for accurate reconstruction of the channel state information (CSI) using few pilot symbols. The proposed novel OMP CS based iterative CE for GFDM in [125] is used for accurate estimation of the CIR so as to precisely reconstruct the interference caused by sub-carriers without added penalty. Simulation results demonstrate that the proposed OMP based CE scheme in [125] efficiently reduces the inherent ISI that is experienced at the receiver of the GFDM system without transmitting power penalty as compared to the existing Tx-IC method developed in [126]. In addition, when simulated using an MMSE receiver, the proposed OMP based CE scheme offers a performance that is almost equivalent to the CRB method proposed in [127]. As a result of the huge demand for the available scarce frequency spectrum, more devices are required to accommodate the improved features such as low-power consumption, low cost and computational complexity. The design improvements are considered in order to enhance the QoS delivery and QoE of network users. However, there is usually manufacturing imperfections that arise due to IQ (inphase (I) and quadrature (Q)) imbalance, which can occur either at the transmitter or receiver front-end. The imbalance consequently results in performance degradation of general wireless communication networks [124]. To reduce the undesired effects of IQ imbalance, training sequence design is investigated in [124]. The training sequence is used for estimating the IQ imbalance parameters on GFDM low complexity receivers over frequency selective channels. This shows an improvement in pilot overhead in comparison to the OFDM based estimation schemes. Moreover, the results demonstrate that the proposed scheme efficiently improves the BER performance of the GFDM based transceivers in comparison to uncompensated cases while providing reliable performances and robustness at extreme IQ imbalance environment.

In [50], a novel CE method is proposed which demonstrates superior performance over conventional LS method when employing several pilot symbols per sub-carrier. The optimal choice of pilot design is analysed for GFDM systems where the performance of different pilot patterns such as block-type and rectangular grid is investigated. It is observed from simulation results that GFDM CE under rectangular grid pilot patterns attains better system performance in comparison to situations where pilots are distributed in different sub-carriers. It is also uncovered from this work [50] that

GFDM demonstrates equivalent performance in comparison with OFDM systems when robust code rates (for instance, 1/3 code rate) are employed while the performance significantly improves at higher code rates (5/6 code rate) as a result of better interference rejection ratio in the GFDM system.

To enhance system performances such as ultra-low latency, low OOB emission, robustness to interference and very high reliability for the emerging next-generation networks, a frequency domain IFPI scheme is developed in [51] for estimating the CIR of non-orthogonal multicarrier systems such as 2×2 MIMO-GFDM system over multipath fading channel with Rayleigh distribution. The performances of OFDM CE is used as a benchmark for analysing the impact of the proposed frequency domain IFPI method on signal properties such as peak-to-average power ratio (PAPR) and power spectral densities (PSD)/OOB emission in comparison to GFDM based transceivers. The results obtained in terms of OOB emission demonstrate that the proposed IFPI GFDM system has slightly OOB emission in comparison to the conventional GFDM signals while windowed GFDM offers equivalent OOB radiation in comparison to the proposed IFPI GFDM. The MSE of this IFPI proposed technique is also compared with conventional OFDM systems and basic GFDM CE. It is observed that the MSE performance of the IFPI technique is identical to that of conventional OFDM as a result of the orthogonality of the pilot symbols to the data symbols. The basic GFDM CE demonstrates a large error floor at high SNR due to the significant effects of interference. The PAPR performance of the basic GFDM is also investigated in comparison to the proposed IFPI GFDM method where it is observed that the PAPR of IFPI GFDM increases due to orthogonal pilot insertion in comparison to basic GFDM.

Pilot-assisted CE is also studied in [52] for MIMO-GFDM systems in the presence of ISI, ICI and inter-antenna interference (IAI) which constitute substantial challenges to the design of the MIMO-GFDM based system. The performance of two known CE schemes (LS and LMMSE) is analysed for pilot-assisted MIMO-GFDM CE in comparison with OFDM systems. The results obtained show that the MSE CE performance of GFDM system contains an error floor resulting from the generated interference precipitating from the data symbols while the MSE is observed to decrease linearly with SNR for OFDM systems. When the CE performance is analysed in terms of SER under OFDM and MIMO-GFDM genie-aided receiver, it is observed (from the obtained results) that the SER of the GFDM system consists of an error floor at higher SNRs as a result of the CE error floor while the SER of OFDM CE proportionally decreases with increase in SNR. The LMMSE estimation which exploits a priori knowledge of channel statistics offered better CE quality in comparison to LS estimation but at high computational complexity. This means that CE for basic GFDM and MIMO-GFDM systems is still an open research area. The performances of semi-blind and blind CE for GFDM system is an open research area that can be evaluated for improving the performances of existing non-orthogonal waveforms for the emerging next generation (5G) networks. In adaptive CE schemes, the parameters of the estimator are updated continuously/adaptively in such a way that the channel and noise statistics are not necessary. The performance analysis of pilot, semi-blind and blind-based adaptive CE schemes for the mentioned potential non-orthogonal waveforms for 5G is another open research problem especially as the signals propagate across highly frequency selective multipath fading communication channels.

4. System Model Description of FBMC OFDM-OQAM and GFDM-OQAM

Filter bank multi-carrier is proposed to be an alternative MCM scheme that improves on the shortcomings of OFDM based systems while emphasis is made on spectral efficiency improvement [10,128]. FBMC systems employ the use of finite impulse response prototype filters that possess longer impulse response than the symbol period (T) [129,130]. In other words, the length of the prototype filter (L_p) is greater than the total number of sub-carriers (M). A higher spectral efficiency is achieved by FBMC based schemes in comparison to CP-OFDM systems because of the absence of CP. In this section, the system model of the FBMC waveforms is analysed assuming NPR and Non-PR prototype filters design. In NPR, the distortion of signals is minimised from an accurate design of

the FIR low-pass prototype filter which subsequently reduces the amplitude distortions. For Non-PR, aliasing and amplitude distortions are more prominent which may reduce system efficacy.

4.1. OFDM-OQAM Transceiver

The conventional stages of the OFDM-OQAM scheme consist of a transmitter, channel and a receiver structure. The OFDM-OQAM structure is made up of the SFB at the transmitter and the AFB at the receiver. Figure 15 depicts the block diagram of a filter bank OFDM-OQAM transceiver. The figure consist of a OQAM pre-processing/post processing, transformation blocks, filtering stage, CE block, and signal conversions blocks. As mentioned above, we review the performance of the filter bank OFDM-OQAM transceiver assuming two filter design conditions: NPR and Non-PR prototype filters design.

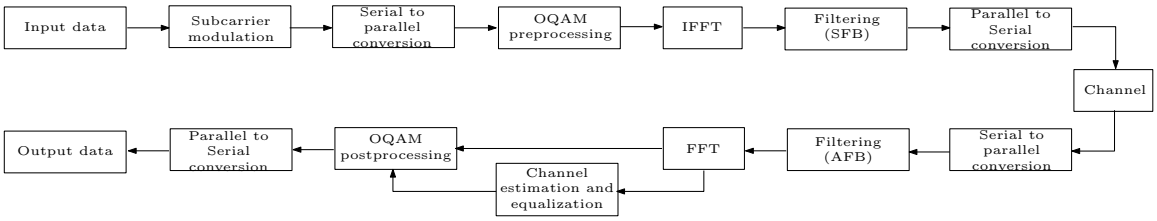

Figure 15. Structure of a filter bank OFDM-OQAM system.

4.1.1. OFDM-OQAM Transceiver: NPR Design

4.1.1.1. Transmitter Description

Consider the OFDM-OQAM transmitter model diagram of Figure 16. The complex QAM symbols at the input $(c[l,k])$ have their real and imaginary parts interleaved by a time offset of $\frac{T}{2}$, where l represents the OQAM preprocessing input/post processing output sample index and n is the OQAM preprocessing output/post processing input sample index while T is the signalling period. After the bits are mapped into symbols, OQAM pre-processing is performed on the QAM symbols where the complex input symbols are mapped into real data symbols $d[n,k]$ at k sub-carrier index (representing the in-phase components of $c[l,k]$) and are transmitted at a rate $\frac{2}{T}$, where $T = \frac{1}{\Delta f}$ and Δf is the sub-carrier spacing. The quadrature components of the input symbols $c[l,k]$ are represented as $d[n+1,k]$ in an entire process termed complex to real conversion (C2R) [123].

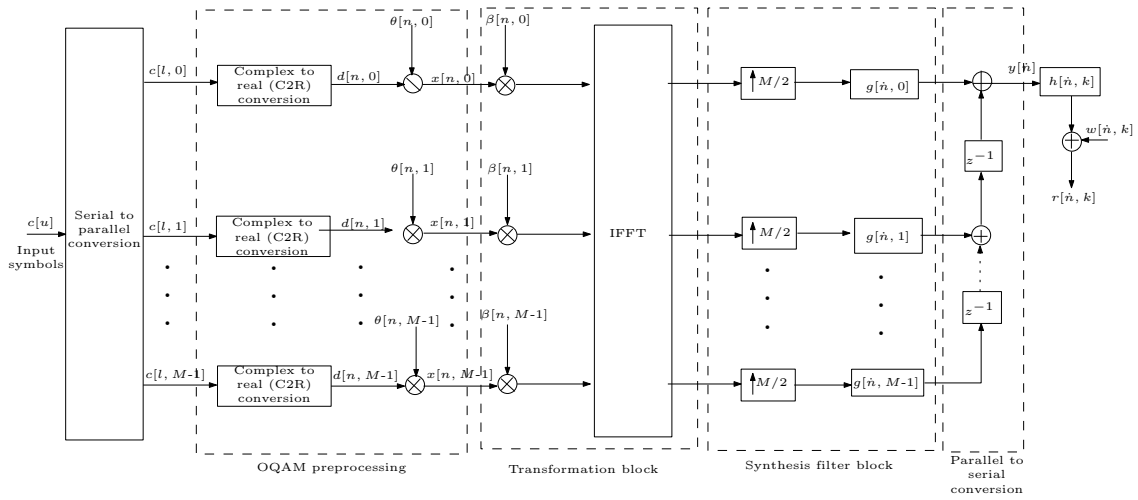

Figure 16. Structure of a filter bank OFDM-OQAM transmitter.

The conversion of the complex input symbols to real symbols is mapped mathematically as [123,131]:

$$d[n,k] = \begin{cases} R_e(c[l,k]); & k \text{ even}, \\ I_m(c[l,k]); & k \text{ odd}. \end{cases} \tag{1a}$$

$$d[n+1,k] = \begin{cases} I_m(c[l,k]); & k \text{ even}, \\ R_e(c[l,k]); & k \text{ odd}. \end{cases} \tag{1b}$$

In Equation (1), the notation R_e and I_m signifies the real and imaginary parts of the complex input symbols, respectively. To ensure orthogonality of sub-carriers, $\theta[n,k]$ is multiplied by $d[n,k]$ resulting in [35,132]:

$$x[n,k] = d[c,k]\theta[n,k], \tag{2}$$

where $x[n,k]$ is the OQAM preprocessing output symbols and $\theta[n,k]$ is defined as:

$$\theta[n,k] = j^{(k+n)}. \tag{3}$$

Before implementing IFFT, $x[n,k]$ undergoes a transformation process where it is multiplied by the beta carrier (β) in order to provide enhanced robustness to the samples as they are been prepared to propagate through the wireless channel. Possible loss of sub-carrier orthogonality due to pulse shaping at SFB is also minimised from this transformation, since the cyclic prefix of the conventional OFDM transceivers are replaced (in FBMC OFDM-OQAM systems) with well-designed prototype filters that have good localisation properties [133], in noth the frequency and time domains. The beta carrier (β) is mathematically given as:

$$\beta[n,k] = (-1)^{kn} exp\left(-j\frac{2\pi k}{M}\left(\frac{L_p-1}{2}\right)\right), \tag{4}$$

where M is the IFFT size or the total number of sub-carriers, k is the sub-carrier index for $k = 0, 1, 2, \ldots, M-1$, and L_p is the length of the FBMC prototype filter $p[n,k]$ given as:

$$L_p = KM. \tag{5}$$

In Equation (5), K is the overlapping factor that determines the number of symbols that superpose each other in time. The use of complex modulated filter banks is employed to ensure high spectral efficiency. The sub-channel synthesis filter bank impulse response $g[\dot{n},k]$ is expressed as [122,123,134]:

$$g[\dot{n},k] = p[\dot{n}] exp\left(j\frac{2\pi k}{M}\left(\dot{n} - \frac{L_p-1}{2}\right)\right), \tag{6}$$

where $\dot{n}$ in Equation (6) is the symbol index at the SFB output and the AFB input for $\dot{n} = 0, 1, 2, \ldots, L_p-1$. To achieve NPR prototype filters, the FIR of the low-pass prototype filter $p[\dot{n}]$ is defined as [123,131,134]:

$$p[\dot{n}] = \tilde{P}[0] + 2\sum_{k=1}^{\frac{L_p-1}{2}} (-1)^k \tilde{P}[k] cos\left(\frac{2\pi k}{KM}\left(\dot{n} + \frac{KM-(L_p-1)}{2}\right)\right), \tag{7}$$

where $w[k] = \frac{2\pi k}{KM}$ is the uniformly spaced frequency points. From Equation (7), $\dot{n} = 0, 1, 2, \ldots, L_p-1$ and $\tilde{P}[0] = 1$. Moreover, $p[\dot{n}]$ is designed such that it meets the condition in Equation (8):

$$\begin{cases} \tilde{P}[0] = 1, \\ \tilde{P}[c]^2 + \tilde{P}[K-c]^2 = 1, \quad \text{for } c = 1, 2, \ldots, \lfloor \frac{K}{2} \rfloor, \\ \tilde{P}[c] = 0 \quad \text{for } c = K, K+1, \ldots, \frac{L_p - 1}{2}, \end{cases} \tag{8}$$

where c= 1, 2, ..., $\lfloor K/2 \rfloor$ and $\tilde{P}[0]$ for $k = K, K+1, ..., \frac{(L_p-1)}{2}$. For this system, the values of $\tilde{P}[c]$ are initialised and designed as shown in Table 5 for different values of overlapping factors.

Table 5. Different values of overlapping factors.

Overlapping Factor (*K*)	**4**				**3**			**2**		**1**
Filter impulse ($\tilde{P}[c]$)	$\tilde{P}[0]$	$\tilde{P}[1]$	$\tilde{P}[2]$	$\tilde{P}[3]$	$\tilde{P}[0]$	$\tilde{P}[1]$	$\tilde{P}[2]$	$\tilde{P}[0]$	$\tilde{P}[1]$	$\tilde{P}[0]$
	1	0.9720	$\frac{\sqrt{2}}{2}$	0.2351	1	0.9114	0.4114	1	$\frac{\sqrt{2}}{2}$	1

Figure 17 illustrates the simulated prototype impulse response $(p[\dot{n}])$ at different overlapping factors (K) using Equation (7). In the figure, it can be observed that, at K = 1, the FBMC scheme adopts the rectangular pulse shaping of OFDM systems.

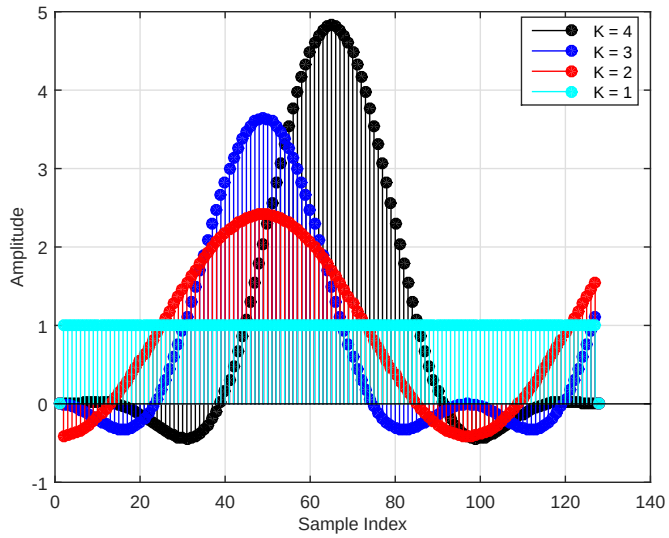

Figure 17. Plot of filter impulse response for different overlapping factor K, M = 32.

4.1.1.2. Channel Description

The frequency domain channel transfer function (FD-CTF) fading coefficients $H[k]$ can be described by two properties: power spectral density (PSD) and the autocorrelation function (ACF). The PSD is expressed by [123]:

$$s|f| = \begin{cases} \frac{1}{\pi f_d \sqrt{1-(f/f_d)^2}}, & |f| \leq f_d \\ 0, & \text{elsewhere.} \end{cases} \tag{9}$$

If L_{ch} represents the length of the channel, then the corresponding normalised discrete-time ACF is expressed by Equation (10) under the assumption that the channel is repeated for a frame [123,135]:

$$a[k] = J_0\left(2\pi f_d T_s \left(\frac{M}{L_{ch}}\right)|k|\right), \quad k = 0, 1, 2, \ldots, (L_{ch} - 1). \tag{10}$$

Equation (9) is the u-shaped band limited Jakes spectrum, where f_d is the maximum Doppler frequency of the moving channel given as $f_d = \frac{v}{\lambda}$. The velocity of the moving mobile is denoted by v, and λ is the wavelength of the carrier wave. A plot of the u-shaped Jakes power spectrum for f_d = $10Hz$ and f_d = $200Hz$ is given in Figure 18. In Equation (10), $J_0(\cdot)$ is the zero-order Bessel function of the first kind, T_s is the symbol period. Note that $f_d T_s$ is normally referred to as the normalised Doppler frequency (Doppler rate).

The correlation matrix $(\mathbf{R}_{HH}[k])$ is given in its expanded form in Equation (11) as a function of ACF as [135,136]:

$$\mathbf{R}_{HH}[k] = \begin{bmatrix} a[0] & a[1] & \dots & a[(L_{ch}-1)] \\ a[1] & a[0] & \dots & a[(L_{ch}-2)] \\ \vdots & \vdots & \ddots & \vdots \\ a[(L_{ch}-1)] & a[(L_{ch}-2)] & \dots & a[0] \end{bmatrix}. \tag{11}$$

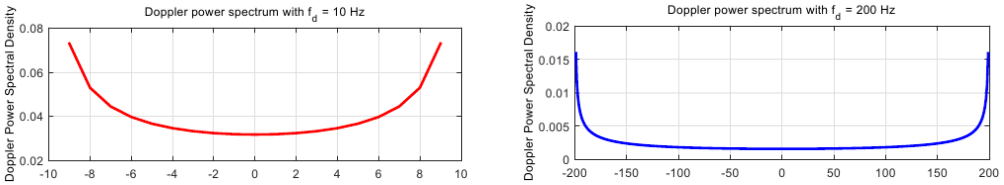

(**a**) f_d = 10 Hz (**b**) f_d = 200 Hz

Figure 18. U-shaped Jakes power spectrum.

The FD-CTF fading channel coefficients $H[k]$ can be generated via an L_{ch}th-order autoregressive (AR) process represented as $AR(L_{ch})$. It can thus be expressed as [123,135,136]:

$$H[k] = \sum_{i=1}^{L_{ch}} z[i]H[k-i] + \Omega[k], \quad k = 0, 1, 2, \dots, (L_{ch}-1), \tag{12}$$

where $H[k]$ represents the channel fading coefficient over the kth sub-carrier. The notation $z[i]$ is given by Equation (13):

$$z[i] = -\varphi[i], \tag{13}$$

and $\varphi[i]$ is defined as:

$$\varphi[i] = \Big[\varphi[1], \varphi[2], \dots, \varphi[L_{ch}]\Big]^T. \tag{14}$$

In Equation (13), T is the transpose operator. Moreover, $\Omega[k]$ in Equation (12) is a zero mean white Gaussian noise process with variance σ^2_Ω given as [135,136]:

$$\sigma^2_\Omega = a[0] + \sum_{k=0}^{L_{ch}-1} \varphi[k]a[k], \tag{15}$$

where $\Omega[k]$ are the coefficients of the AR model parameters and can be obtained by computing the Yule–Walker (YW) equation defined by Equations (16) and (17).

$$\varphi[k] = -R^{-1}_{HH}[k]b[k], \tag{16}$$

$$b[k] = \Big[a[0], a[1], \dots, a[L_{ch}-1]\Big]^T. \tag{17}$$

Based on the channel expression in Equation (12), the channel coefficients are realised to be equal for a given frame length $F_L = \frac{M}{L_{ch}}$. For instance, the fading coefficients at $H[0]$ is given as:

$$H[0] = z[1]H[-1] + \Omega[0], \tag{18}$$

where $H[-1]$ in Equation (18) is initialised through random generation. The channel coefficients across all frequencies at a given time for $F_L = \frac{M}{L_{ch}}$ are chosen to be the same for all M sub-carriers. For example, if $\dot{H}[\ddot{k}]$ represents the channel coefficients across the $\ddot{k}$th sub-carrier for $\ddot{k} = 0, 1, \ldots, M-1$, then $\dot{H}[0]$ to $\dot{H}[F_L - 1]$ are chosen to equal the $H[0]$ obtained from Equation (12).

4.1.1.3. Receiver Description

After passing through the fading channel under NPR conditions, the received signal as represented in Figure 19 over the kth sub-carrier is given by [10]:

$$s[n,k] = \ddot{\mathbf{H}}x[n,k] + \eta[n,k], \tag{19}$$

where $\ddot{\mathbf{H}}$ is an $M \times M$ diagonal matrix that contains the fading channel coefficients $\dot{H}[\ddot{k}]$, and $\eta[n,k]$ is a Gaussian noise process with variance σ_η^2 expressed by:

$$\eta[n,k] = w[n,k] * f[\dot{n},k]. \tag{20}$$

The expression $w[n,k]$ in Equation (20) signifies the mutually independent zero-mean complex AWGN process with equal variances $(\sigma_{w,k}^2)$. In addition, the variance of η $(\sigma_{\eta,k}^2)$ is given as:

$$\sigma_{\eta,k}^2 = \sigma_{w,k}^2 \sum_{j=0}^{L_p-1} f^2[j,k], \tag{21}$$

while the receiver AFB impulse response is defined as [131,134]:

$$f[\dot{n},k] = g^*[(L_p - 1 - \dot{n}),k]. \tag{22}$$

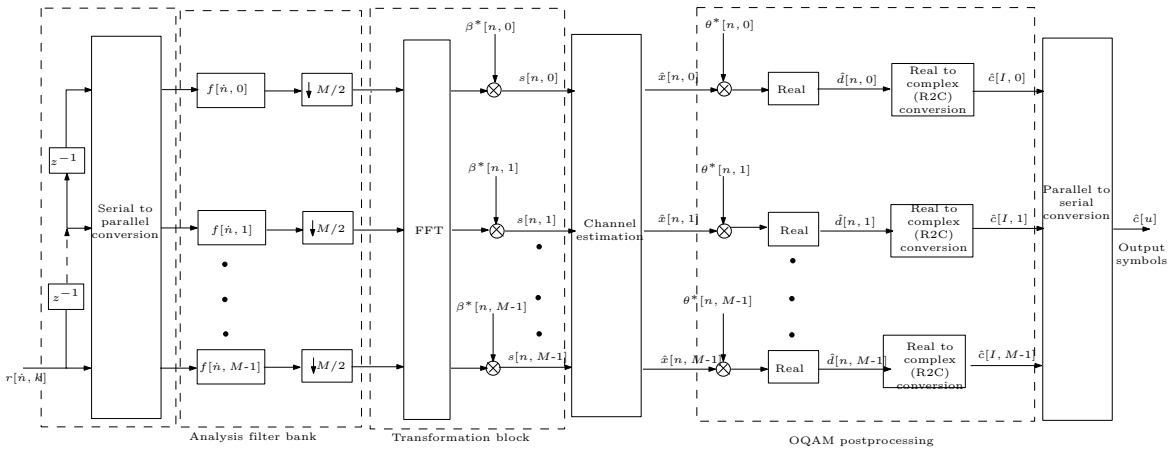

Figure 19. Structure of filter bank OFDM-OQAM receiver.

4.1.2. OFDM-OQAM Transceiver: Non-PR design

Transmitter Description

In Non-PR conditions of filter banks, the impulse response of the AFB FIR prototype filter is different from that of the SFB. In Non-PR filter design, the analysis filter bank is not directly

a time-reversed version of the corresponding synthesis filter bank due to the difference in prototype filter impulse response $\acute{p}[\dot{n}]$. To achieve this imperfection, an error $\bar{\delta}$ is randomly introduced to the analysis filter FIR prototype filter such that $-\bar{\Delta} < \bar{\delta} < +\bar{\Delta}$, where $\bar{\Delta} = 0.1$. Hence, the filter bank prototype filter according to Equation (7) is modified by the introduction of an error ($\delta[k]$) so as to yield the non-perfect reconstructed FIR analysis prototype filter bank formulated in Equation (23).

$$\acute{p}[\dot{n}] = \tilde{P}[0] + 2\sum_{k=1}^{\frac{L_p-1}{2}}(-1)^k(\tilde{P}[k] + \bar{\delta}[k])cos\left(\frac{2\pi k}{KM}\left(\dot{n} + \frac{KM-(L_p-1)}{2}\right)\right) \tag{23}$$

The transmitted filtered OFDM-OQAM symbol $y[\dot{n},k]$ over the kth sub-carrier for the $\dot{n}$th symbol, assuming Non-PR, is obtained by convolving the synthesis filter bank impulse response $(g[\dot{n},k])$ with the up sampled transmitted signal $(x[\dot{n},k])$ as:

$$y[\dot{n},k] = (x[\dot{n},k] * g[\dot{n},k]) = \sum_{l=0}^{L_p-1} x[\dot{n}-l,k]g(l,k) \tag{24}$$

Channel Description

The channel assuming Non-PR is modelled in a similar way to the channel model presented in Section 4.1.1.2.

Receiver Description

Since the analysis filter bank is not directly a time-reversed version of the corresponding synthesis filter bank, the analysis filter bank impulse response $(\acute{f}[\dot{n},k])$ obtained from the introduction of error is:

$$\acute{f}[\dot{n},k] = \acute{p}[\dot{n}]exp\left(j\frac{2\pi k}{M}\left(\dot{n} - \frac{(L_p-1)}{2}\right)\right). \tag{25}$$

The $\dot{n}$th filter bank OFDM-OQAM symbol received over the kth sub-carrier is therefore given as [29]:

$$r[\dot{n},k] = y[\dot{n},k]h[\dot{n},k] + w[\dot{n},k]. \tag{26}$$

In Equation (26), $h[\dot{n},k]$ is the frequency selective Rayleigh fading channel impulse response and $w[\dot{n},k]$ signifies the mutually independent zero-mean complex AWGN process with variance $\sigma^2_{w,k}$ given as:

$$\sigma^2_{w,k} = E\left[x^2[\dot{n},k]\right]10^{\frac{-\gamma_{dB}}{10}}. \tag{27}$$

The received signal $s[n,k]$, after $r[\dot{n},k]$ has been processed with the filter bank, is given as [2]:

$$s[n,k] = \left[r[\dot{n},k] * \acute{f}[\dot{n},k]\right]_{\downarrow\frac{M}{2}}, \tag{28}$$

$$s[n,k] = \left[x[\dot{n},k]q[\dot{n},k] + \eta[\dot{n},k]\right]_{\downarrow\frac{M}{2}}, \tag{29}$$

where

$$q[\dot{n},k] = \left[h[\dot{n},k]g[\dot{n},k] * \acute{f}[\dot{n},k]\right], \tag{30}$$

and $\eta[\dot{n},k]$ in Equation (29) is a Gaussian noise process expressed by:

$$\eta[\dot{n},k] = \left[w[\dot{n},k] * \acute{f}[\dot{n},k]\right]. \tag{31}$$

4.1.3. Channel Estimation for OFDM-OQAM

The performances of two linear and three adaptive based CE algorithms are analysed for the described filter bank OFDM-OQAM based transceiver. These linear algorithms are LS and LMMSE, and the adaptive estimation schemes are LMS, normalised LMS (NLMS) and recursive LS (RLS).

Least Square

The LS channel estimate is given as [100]:

$$\begin{aligned}\hat{\mathbf{H}}_{LS}[n,k] &= \left[\hat{H}_{LS}[n,0], \hat{H}_{LS}[n,1], \ldots, \hat{H}_{LS}[n,(L_{ch}-1)]\right]^T \\ &= \left[\frac{L_{ch}}{M}\left(\sum_{k=0}^{\frac{M}{L_{ch}}-1}\frac{s[n,k]}{x[n,k]}, \sum_{k=ML_{ch}}^{\frac{2M}{L_{ch}}-1}\frac{s[n,k]}{x[n,k]}, \ldots\ldots, \sum_{k=M(L_{ch}-1)L_{ch}}^{M-1}\frac{s[n,k]}{x[n,k]}\right)\right]^T.\end{aligned} \tag{32}$$

LMMSE

The simplified LMMSE channel estimate $\hat{\mathbf{H}}_{LMMSE}[n,k]$ is generally given as [73,86,137]:

$$\hat{\mathbf{H}}_{LMMSE}[n,k] = \mathbf{R}_{Hs}[n,k]\mathbf{R}_{ss}^{-1}[n,k]s[n,k], \tag{33}$$

where $\mathbf{R}_{Hs}[n,k]$ is the cross-covariance matrix between $H[n,k]$ and $s[n,k]$ expressed as:

$$\mathbf{R}_{Hs}[n,k] = E[Hs^H] = \mathbf{R}_{HH}[n,k]\mathbf{X}^H[n,k], \tag{34}$$

and $\mathbf{R}_{ss}[n,k]$ is the auto-covariance matrix of $s[n,k]$ expressed as:

$$\mathbf{R}_{ss}[n,k] = E[ss^H] = \mathbf{X}[n,k]\mathbf{R}_{hh}[n,k]\mathbf{X}^H[n,k] + \sigma_\eta^2\mathbf{I}[m]. \tag{35}$$

In Equation (34), $\mathbf{X}[n,k] = diag[\mathbf{x}[n,k]]$. Therefore, substituting Equations (34) and (35) into Equation (33) gives:

$$\hat{\mathbf{H}}_{LMMSE}[n,k] = \frac{\mathbf{R}_{HH}[n,k]s[n,k]}{\mathbf{X}[n,k]\left[\mathbf{R}_{HH}[n,k] + (\mathbf{X}^H[n,k]\mathbf{X}[n,k])^{-1}\sigma_\eta^2\mathbf{I}[n,k]\right]}, \tag{36}$$

where $\mathbf{R}_{HH}$ is the autocorrelation matrix of the channel impulse response given by Equation (11). The notation σ_η^2 denotes the noise variance $E|\eta[n,k]|^2$ defined in Equation (21), $\mathbf{I}[n,k]$ is an identity matrix, and E is the expectation notation.

Least Mean Square

This cost function to be minimised for LMS based CE is expressed as [19,136,138,139]:

$$\mathbf{J}(\mathbf{n}) = E\{|\mathbf{e}[n,k]|^2\} = E\{\mathbf{e}[n,k]\mathbf{e}^*[n,k]\} \tag{37}$$

where $E\{\cdot\}$ is the expectation operator, $*$ denotes complex conjugation, and $e^*[n,k]$ is the CE error given as:

$$\mathbf{e}^*[n,k] = s^*[n,k] - \hat{H}[n,k]x^H[n,k]. \tag{38}$$

The LMS for the filter bank OFDM-OQAM system is given as:

$$\hat{\mathbf{H}}_{LMS}[n+1,k] = \hat{H}[n,k] + \mu\mathbf{e}^*[n,k]x[n,k], \tag{39}$$

where μ is the fixed positive step size parameter that satisfies the condition $0 < \mu < 2$.

Normalised Least Mean Square

In NLMS CE, the estimation error is normalised by the power of the input signal. The CIR for this algorithm is represented as [136–140]:

$$\hat{\mathbf{H}}_{NLMS}[n+1,k] = \hat{H}[n,k] + \frac{\mu \mathbf{e}^*[n,k]x[n,k])}{||x[n,k]||^2}, \tag{40}$$

where $||x[n,k]||^2$ represents the Euclidean norm of the staggered input OQAM symbols, μ is the step size parameter and the error $e^*[n,k]$ is expressed as in Equation (38).

Recursive Least Square

The index of performance to be minimised for RLS is [136,141]:

$$\mathbf{J}(\mathbf{n}) = \sum_{k=0}^{n-1} \lambda^{n-k} |\mathbf{e}[n,k]|^2, \tag{41}$$

where λ is the forgetting/weighting factor, which assumes value in the range $0 << \lambda < 1$. The inverse autocorrelation matrix ($\mathbf{R}^{-1}[n,k]$) of input vector $x[n,k]$ is given as:

$$\mathbf{R}^{-1}[n,k] = \lambda^{-1}\mathbf{R}^{-1}[n-1,k] - \lambda^{-1}\tilde{\mathbf{g}}[n,k]x^H[n,k]\mathbf{R}^{-1}[n-1,k], \tag{42}$$

where $\tilde{\mathbf{g}}[n,k]$ is the gain vector expressed as:

$$\tilde{\mathbf{g}}[n,k] = \frac{\lambda^{-1}\mathbf{R}^{-1}[n-1,k]x[n,k]}{1 + x^H[n,k]\lambda^{-1}\mathbf{R}^{-1}[n-1,k]x[n,k]}. \tag{43}$$

Therefore, the RLS channel estimate can be expressed as:

$$\hat{\mathbf{H}}_{RLS}[n,k] = \hat{H}[n-1,k] + \tilde{\mathbf{g}}[n,k]\mathbf{e}^*[n,k], \tag{44}$$

where $\mathbf{e}^*[n,k]$ is defined by Equation (38).

4.2. GFDM-OQAM Transceiver

GFDM is considered to be the most promising candidate for the air interface of 5G networks [142,143]. One of the most distinguishing characteristics of this system is the introduction of flexible pulse shaping across each individual sub-carrier [143]. The filtering of these sub-carriers by well-designed prototype filters reduces the harmful effects of ICI while providing robustness to the system against synchronisation errors [144–146].

GFDM introduces the CP extension properties of OFDM to combat ICI as well as well-designed pulse shaping [147,148]. However, the modulation of each sub-carrier by non-rectangular pulse shaped filters lead to non-orthogonality of sub-carriers in GFDM based schemes [131]. Due to this non-orthogonal nature of the GFDM based system, ISI and ICI are expected to occur whose effects can be mitigated by exploiting the near orthogonality properties of the offset QAM scheme. This paper reviews the GFDM scheme based on OQAM (GFDM-OQAM). Note, to the best of our knowledge, the performance of the GFDM assuming OQAM as the underlying modulation scheme is evaluated in this paper for the first time adopting different existing CE schemes. Moreover, we explain in this paper how to combat the expected detrimental effects of ISI and ICI where each sub-carrier block is modulated against real-valued symbols, unlike the sub-carrier modulation of the complex-valued symbols of GFDM-QAM based systems.

4.2.1. System Description of GFDM-OQAM Transceiver

4.2.1.1. Transmitter Description

Figure 20 depicts a typical GFDM-OQAM system. In GFDM-OQAM based transceivers, the real valued N data symbols generated at the transmitter are decomposed into $\ddot{M}$ sub-symbols, where the sub-symbols are being carried by a sub-carrier [149]. If $\acute{K}$ represents the total number of sub-carriers and $\ddot{M}$ is the total number of sub-symbols per-sub-carrier, then the total number of data symbols to be transmitted is given as:

$$N = \acute{K}\ddot{M}. \tag{45}$$

To implement OQAM for GFDM, let $\vec{\vec{d}}_{\acute{k},\dot{m}}$ represent the real data obtained from the QAM symbols, where $\dot{m}$ is the sub-symbol index at the $\acute{k}$th sub-carrier of the GFDM-OQAM system, the entire symbols to be transmitted can be collected into a vector $\vec{\vec{\mathbf{d}}}$ given as [37]:

$$\vec{\vec{\mathbf{d}}} = [\vec{\vec{d}}_{0,0}, \vec{\vec{d}}_{1,0}, \ldots, \vec{\vec{d}}_{\acute{K}-1,0}, \vec{\vec{d}}_{0,1}, \vec{\vec{d}}_{1,0}, \ldots, \vec{\vec{d}}_{\acute{K}-1,1}, \ldots, \vec{\vec{d}}_{0,\ddot{M}-1}, \vec{\vec{d}}_{\acute{K}-1,\ddot{M}-1}]^T, \tag{46}$$

for $\acute{k} = 0, 1, \ldots, (\acute{K}-1)$ and $\dot{m} = 0, 1, \ldots, \ddot{M}-1$. Each $\vec{\vec{d}}_{\acute{k},\dot{m}}$ symbol of the GFDM system is transmitted with a corresponding pulse shape given as [150]:

$$g_{\acute{k},\dot{m}}[n] = p\left[n - \frac{\dot{m}\acute{K}}{2} mod \acute{K}\ddot{M}\right] exp\left(j\frac{2\pi\acute{k}}{\acute{K}}\left(n - \frac{(L_p-1)}{2}\right)\right), \tag{47}$$

where $n = 0, 1, \ldots, N-1$ and $g_{\acute{k},\dot{m}}[n]$ is the shifted version of the prototype filter p in the time and frequency domains as defined in Equation (7) and L_p is the prototype filter length given by Equation (5). Thus, the time domain transmit signal just before cyclic prefix insertion is given as:

$$x[n] = \sum_{\acute{k}=0}^{\acute{K}-1} \sum_{\dot{m}=0}^{\ddot{M}-1} \vec{\vec{d}}_{\acute{k},\dot{m}} g_{\acute{k},\dot{m}}[n] e^{j\phi_{\acute{k},\dot{m}}}, \tag{48}$$

where $e^{j\phi_{\acute{k},\dot{m}}}$ is used to ensure a $\frac{\pi}{2}$ difference in phase between the real valued data $\vec{\vec{d}}_{\acute{k},\dot{m}}$ in time and frequency domains, and $\phi_{\acute{k},\dot{m}}$ is given as in Equation (49).

$$\phi_{\acute{k},\dot{m}} = \frac{(\acute{k}+\dot{m})\pi}{2}. \tag{49}$$

The operations described in this Section 4.2.1.1, can be written in a matrix form $(\vec{\vec{x}})$ given as $\vec{\vec{x}} = \mathbf{A}\vec{\vec{\mathbf{d}}}$ [151], where $\vec{\vec{\mathbf{d}}}$ is given in Equation (40), and $\mathbf{A}$ is an $N \times N$ transmitter modulation matrix containing elements of $g_{\acute{k},\dot{m}}[n]$ expressed as:

$$\mathbf{A} = [\mathbf{g}_{0,0}, \ldots, \mathbf{g}_{\acute{K}-1,0}, \mathbf{g}_{0,1}, \mathbf{g}_{1,1}, \ldots, \mathbf{g}_{\acute{K}-1,1}, \cdots, \mathbf{g}_{0,\ddot{M}-1}, \mathbf{g}_{1,\ddot{M}-1}, \cdots \mathbf{g}_{\acute{K}-1,\ddot{M}-1}]. \tag{50}$$

where $\mathbf{g}_{\acute{k},\dot{m}}$ are vectors given as $\mathbf{g}_{\acute{k},\dot{m}} = \left[g_{\acute{k},\dot{m}[n]} e^{j\phi_{\acute{k},\dot{m}}}\right]^T$. Cyclic prefix of length N_{CP} is then appended to $\vec{\vec{x}}$ so as to obtain the final transmit signal $\vec{\vec{x}}_T$ whose length is $(N + N_{CP})$.

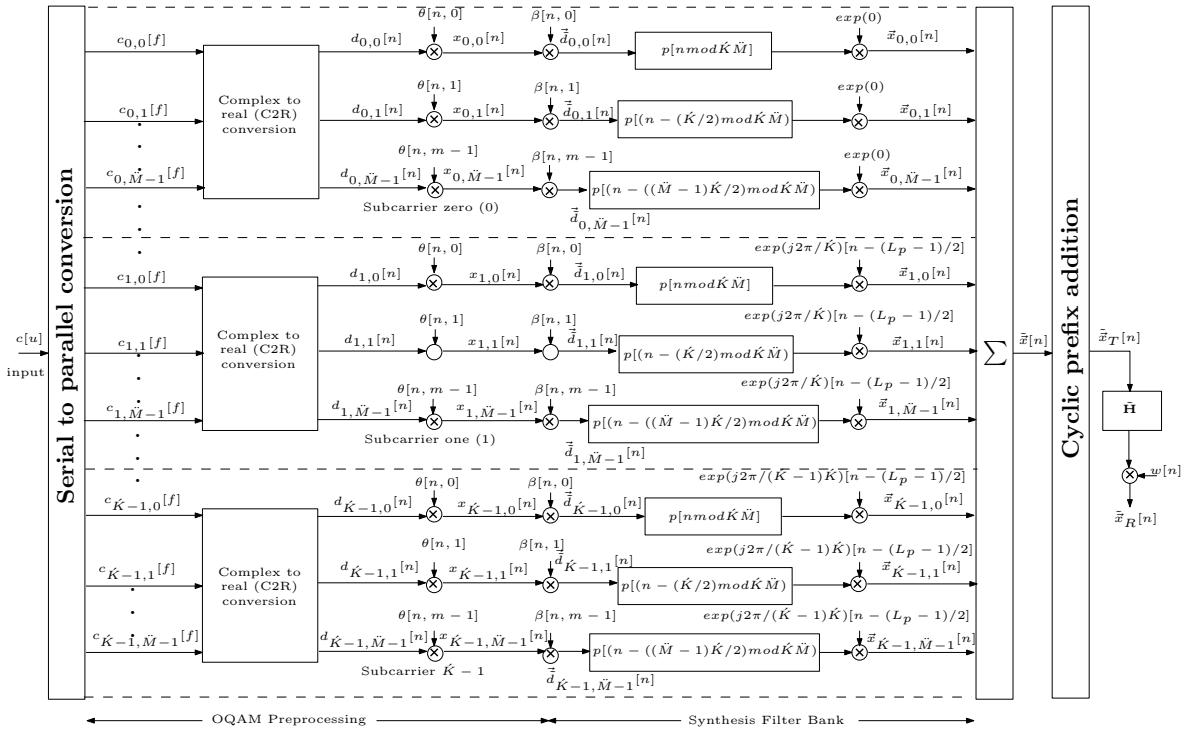

Figure 20. Structure of GFDM-OQAM based transmitter.

4.2.1.2. Channel Description

The channel is modelled similarly to the Rayleigh fading channel described in Section 4.1.1.2. However, the channel frequency coefficients are realised such that they have L_{ch} different values, that is, $H[\acute{k}]$= $\Big[H[0], H[1], \ldots, H[L_c h - 1]\Big]$. This is then converted into the time domain channel impulse response $h(\acute{n})$ through the use of IDFT as:

$$h(\acute{n}) = IDFT[H[\acute{k}]] = \sum_{\acute{k}=0}^{\acute{L}_{ch}-1} H[\acute{k}] e^{j\frac{2\pi \acute{k}\acute{n}}{N}} \quad \text{for} \quad \acute{n} = 0, 1, \ldots, L_{ch} - 1. \tag{51}$$

4.2.1.3. Receiver Description

After the transmitted symbols have propagated through the wireless channel, the received signal can be expressed as:

$$\tilde{\vec{x}}_R[n] = \tilde{\mathbf{H}} \tilde{\vec{x}}_T[n] + w[n], \tag{52}$$

where $\tilde{\vec{x}}_T[n]$ is the transmitted signal with CP. If the CP is removed, the received signal is denoted as $\vec{x}_R[n]$. The symbol $w[n]$ in Equation (52) is the complex AWGN vector with zero mean and variance σ_w^2. The notation $\tilde{\mathbf{H}}$ ($\tilde{\mathbf{H}} = circ(h(\acute{n}))$) is the circulant channel matrix (CCM) having a band diagonal structure based on the channel impulse responses obtained from Equation (51) and it is obtained as described in Algorithm 1.

Algorithm 1: Sequential procedure for realising the GFDM-OQAM CCM.

Input: $\{L_{ch}, \acute{K}, \ddot{M}, N_{cp}.\}$

Output: $\left\{\tilde{\tilde{\mathbf{H}}}\right\}$.

01 Compute $N = \acute{K}\,\ddot{M}$;

02 Generate $H[\acute{K}]$ vector using Equation (12), where length of $H[\acute{K}] = L_{ch}$;

03 Compute $h(\acute{n}) = \text{ifft}(H[\acute{K}])$ according to Equation (51);

04 Generate $\tilde{\tilde{\mathbf{H}}} = \text{zeros}\Big((N + N_{cp}), (N + N_{cp})\Big)$;

05 Compute $\tilde{\tilde{\mathbf{H}}}(1, [1 : L_{ch}]) = h(\acute{n})$;

06 for ii $\rightarrow 1 : 1 : (size(\tilde{\tilde{\mathbf{H}}}, 2) - 1)$;

07 $\tilde{\tilde{\mathbf{H}}}(ii + 1, 1) = \tilde{\tilde{\mathbf{H}}}(ii, end)$;

08 $\tilde{\tilde{\mathbf{H}}}(ii + 1, [2 : end]) = \tilde{\tilde{\mathbf{H}}}(ii, [1 : end - 1])$;

09 end for (in line 06);

10 return $\left\{\tilde{\tilde{\mathbf{H}}}\right\}$.

Therefore, the received signal after equalisation is given as:

$$x_R[n] = \vec{x}_R[n] H^{-1}_{chan}[n], \tag{53}$$

where H is the Hermitian transpose operator and $H_{chan}[n]$ are the fading coefficients obtained from the CE. Thus, the demodulated signal is given as:

$$c_R[n] = \mathbf{B} x_R[n], \tag{54}$$

where $\mathbf{B}$ is the matched filter receiver matrix given as $\mathbf{B} = \mathbf{A}^H$, and $\mathbf{A}$ is the $N \times N$ transmitter modulation matrix.

4.2.2. Channel Estimation for GFDM-OQAM

To avoid harping on, the linear CE techniques for the described filter bank GFDM-OQAM based transceiver is only presented in this section. The adaptive schemes can be derived in similar procedures as mentioned in Section 4.1.3.

Least Square

The GFDM-OQAM LS channel estimate is given as:

$$\begin{aligned} \hat{\mathbf{h}}_{LS}[\acute{n}, \acute{k}] &= \Big[\hat{h}_{LS}[\acute{n}, 0], \hat{h}_{LS}[\acute{n}, 1], \ldots, \hat{h}_{LS}[\acute{n}, (L_{ch} - 1)]\Big]^T \\ &= \left[\frac{L_{ch}}{M}\left(\sum_{\acute{k}=0}^{\frac{M}{L_{ch}}-1} \frac{\vec{x}_R[\acute{n}, \acute{k}]}{\tilde{\vec{x}}[\acute{n}, \acute{k}]}, \sum_{\frac{k=M}{L_{ch}}}^{\frac{2M}{L_{ch}}-1} \frac{\vec{x}_R[\acute{n}, \acute{k}]}{\tilde{\vec{x}}[\acute{n}, \acute{k}]}, \ldots\ldots, \sum_{\frac{k=M(L_{ch}-1)}{L_{ch}}}^{M-1} \frac{\vec{x}_R[\acute{n}, \acute{k}]}{\tilde{\vec{x}}[\acute{n}, \acute{k}]}\right)\right]^T. \end{aligned} \tag{55}$$

LMMSE

The simplified time-domain LMMSE channel estimate $\hat{\mathbf{h}}_{LMMSE}[\acute{n}, \acute{k}]$ for GFDM-OQAM is given as [73,86,137]:

$$\hat{\mathbf{h}}_{LMMSE}[\acute{n}, \acute{k}] = \frac{\mathbf{R}_{HH}[\acute{k}] \vec{x}_R[\acute{n}, \acute{k}]}{\mathbf{X}[\acute{n}, \acute{k}]\left[\mathbf{R}_{HH}[\acute{k}] + (\mathbf{X}^H[\acute{n}, \acute{k}]\mathbf{X}[\acute{n}, \acute{k}])^{-1}\sigma^2_{\acute{\eta}}\mathbf{I}[\acute{n}, \acute{k}]\right]}, \tag{56}$$

where $\mathbf{R}_{HH}[\acute{k}]$ is the autocorrelation matrix of the channel impulse response given by Equation (11), σ_{η}^{2} denotes the noise variance $E|\eta[n,k]|^2$ defined in Equation (21), $\mathbf{I}[n,k]$ is an identity matrix and E is the expectation notation.

5. Simulations and Discussion of Results

All simulations reported in this paper were implemented using MATLAB programming language. Simulations for the filter bank OFDM-OQAM were implemented assuming NPR and Non-PR based on the system model described in Figures 16 and 19. Firstly, we show the plot comparing the FIR of the prototype filter assuming NPR and Non-PR, as shown in Figure 21.

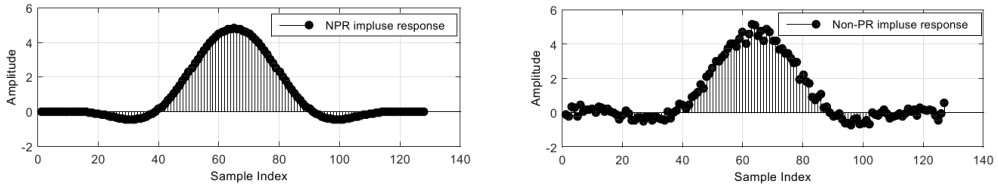

(**a**) NPR (**b**) Non-PR

Figure 21. Filter impulse responses.

Thus, the performances of the linear and adaptive estimators are analysed and compared with one another through Monte-Carlo simulations with 10,000 trials per SNR. Uncoded 16-QAM scheme is assumed for the OFDM-OQAM based transceiver with M = 512 sub-carriers under frequency selective Rayleigh fading channel with Doppler rates $f_d T_s$ = 0.001 and $f_d T_s$ = 0.02, corresponding to both slow and fast fading channel conditions, respectively. The speed of the moving mobile is selected as 360 km/h and 18 km/h, correlating with fast and slow channels, respectively. The overlapping factor is chosen as K = 4, while the initial value of the filter coefficient $P[k]$ is selected to be $\tilde{P}[1]$ = 0.97195983 [131]. Cyclic prefix overhead is not considered for the OFDM-OQAM system in contrast to the GFDM-OQAM system.

In a similar procedure, using similar parameters as summarised in Table 6, the GFDM-OQAM is implemented with the addition of CP overhead of 25% of symbol duration for NPR filter bank. For the adaptive CE algorithms, the positive step size parameter is selected as μ = 0.35 and a regularisation factor δ = 0.001 is chosen to initialise the inverse autocorrelation matrix of Equation (42). Additionally, a forgetting factor λ = 0.998 is selected in the simulation as it is verified in [152] that this value yields a good results.

The results are shown in terms of the NMSE at various levels of SNR. For the Non-PR simulations, the randomly introduced errors with values between -0.1 and 0.1 are chosen to inject imperfection, as shown in Equation (23). Figure 22 demonstrates the curve at 5 dB SNR for the NMSE vs Non-PR error at different values of random errors. It can be seen from the figure that the higher the error value, the more the distortions and degradation in NMSE performance. Moreover, the RLS estimator offers the best performance in comparison with the other estimators, even for high error value of 1.5. Performance comparison in terms of the NMSE versus SNR assuming filter bank OFDM-OQAM under NPR and Non-PR for both slow and fast fading channel is shown in Figure 23a,b. Note that the ideal channel condition is used as a reference point to evaluate the performances of other CE algorithms. In Figure 23a, all CE schemes perform better assuming NPR filter design in comparison to Non-PR filter design. This is largely due to the random errors introduced in the Non-PR filter design. Furthermore, the superior performance of the adaptive schemes over the linear schemes is also demonstrated with RLS showing the best system performance. In Figure 23b, the performance of all the estimators plummets due to the increase in the fading rate ($f_d T_s$). In all practical scenarios, increase in the fading rate automatically reduces the performance of any estimator, as also shown in Figure 23b. This is because the channel fading distortion is more difficult to track in a fast fading channel. As such, there are irregularities in the channel estimate.

Table 6. Simulation parameters for FBMC-OQAM waveforms.

Parameters	Specification	
	OFDM-OQAM	**GFDM-OQAM**
No. of Sub-carriers	512	512
Signal Constellation	16-QAM-OQAM	16-QAM-OQAM
Sampling Frequency	10,000 Hz	10,000 Hz
Doppler Frequency	10 and 200 (Hz)	10 and 200 (Hz)
Sampling Rate	$\frac{1}{10^4}s$	$\frac{1}{10^4}s$
Doppler Rate(s)	0.001 and 0.02	0.001 and 0.02
Overlapping Factor	4	4
Filter Coefficient ($\tilde{P}[1]$)	0.97195983	0.97195983
Channel Type	Rayleigh fading	Rayleigh fading
Cyclic Prefix Overhead	–	25%

As mentioned above, we also present the NMSE versus SNR performance comparisons for GFDM-OQAM system assuming both NPR and Non-PR conditions. Figure 24a,b depicts the NMSE versus SNR performance for $f_d T_s = 0.001$ and $f_d T_s = 0.02$, respectively, assuming NPR condition. In the figures, the RLS CE offers the best performance in comparison with the other estimators. Besides, the adaptive estimators exhibit better performance as compared with the linear estimators. In particular, the performance of the linear estimators drops rapidly as the fading rate increases. Likewise, we present the performance comparison of the estimators assuming Non-PR condition, as depicted in Figure 25a,b. In a similar trend, the RLS CE scheme demonstrates the best performance as compared with the other estimators. In addition, all the adaptive CE schemes offer better performance in comparison with the linear CE schemes. Moreover, comparing the NPR filter design performance curves (Figure 24a,b) with the performance curve of the Non-PR filter design (Figure 25a,b) for the GFDM-OQAM system set-up, we observe that the CE schemes offer better performance when the NPR filter design is assumed.

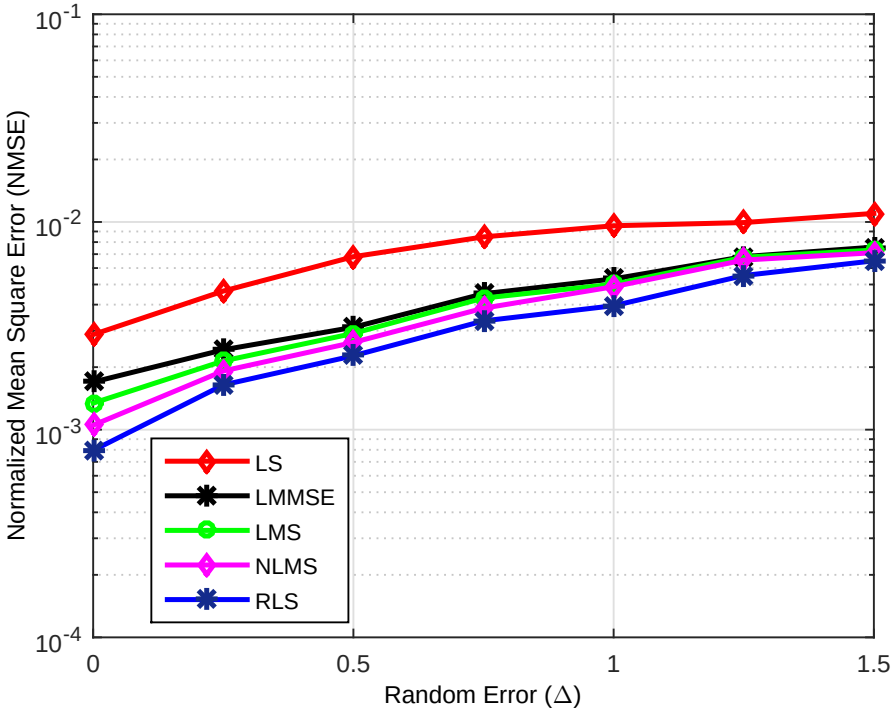

Figure 22. Performance comparison in terms of NMSE versus Non-PR error at SNR = 5 dB.

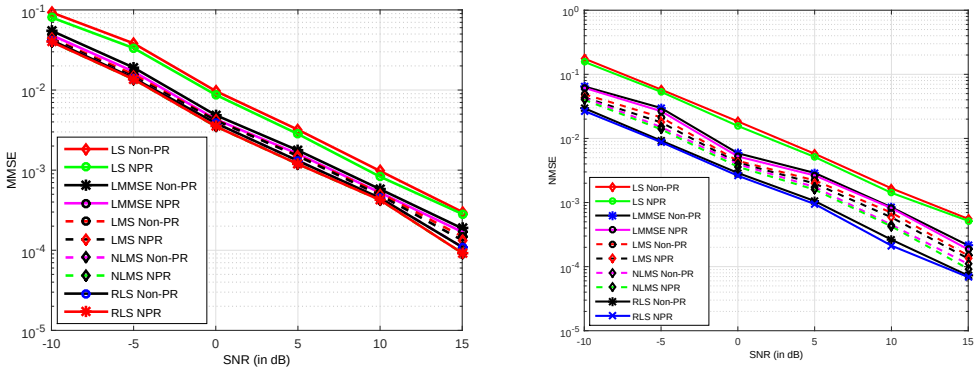

(**a**) $f_d T_s = 0.001$ (**b**) $f_d T_s = 0.02$

Figure 23. Estimators performance comparison in terms of NMSE versus SNR.

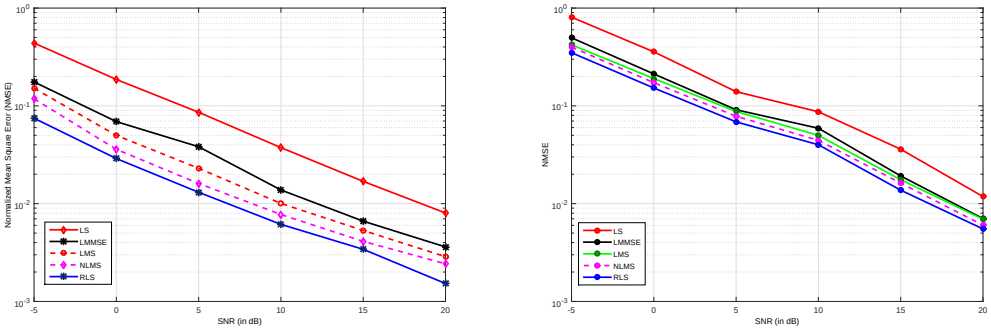

(**a**) $f_d T_s = 0.001$ (**b**) $f_d T_s = 0.02$

Figure 24. Estimators performance comparison in terms of NMSE versus SNR: NPR filter design.

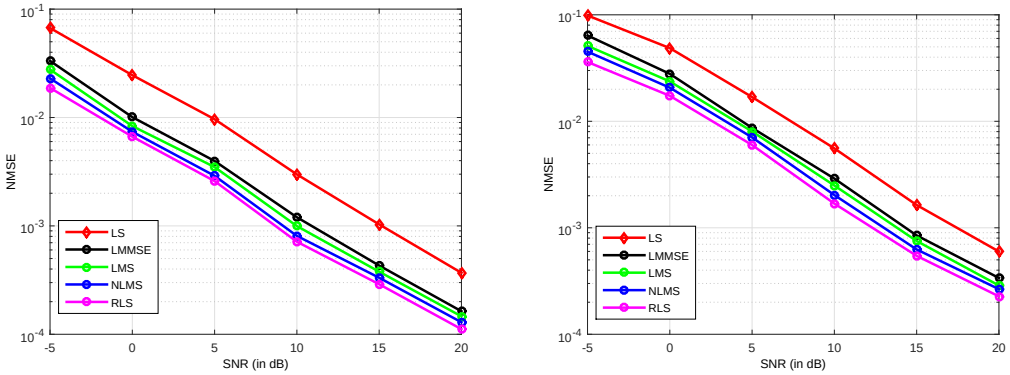

(**a**) $f_d T_s = 0.001$ (**b**) $f_d T_s = 0.02$

Figure 25. Estimators performance comparison in terms of NMSE versus SNR: Non-PR filter design.

6. Findings and Possible Research Directions

Channel estimation is an integral part of general wireless communication systems, most especially, with the emerging 5G technologies. The f-OFDM, filter bank OFDM-OQAM, BFDM, UFMC and GFDM-OQAM based transceivers are identified as suitable modulation schemes for the currently evolving xG of wireless networks. However, the varying nature of the communication channel has been a major challenge to the use of these aforementioned filter bank based transceivers. Different research works are currently ongoing in order to estimate the fading channel characteristics of these transceivers, thereby providing effective and reliable solutions to the use of FBMC based schemes. Extensive research

works have been carried out to estimate the channel fading features when adopting CP-OFDM and SC-FDMA transmission technologies as the underlying modulation schemes (including filter bank based OFDM-OQAM systems); nevertheless, little or no work has been done using GFDM-OQAM as the underlying modulation scheme in the FBMC system. In fact, very little research work has been carried out in this area in terms of developing novel algorithms for estimating the channel fading. GFDM-OQAM is considered to be one of the most promising candidate for the air interface of 5G networks. As such, CE for filter bank GFDM-OQAM (with particular reference to semi-blind and blind techniques) is still an open area for further research, in order to aid this modulation scheme to attain its full potential. Although this paper reviews the performances of filter bank OFDM and GFDM based schemes for two linear and three adaptive CE schemes assuming OFDM-OQAM and GFDM-OQAM as the underlying modulation, we emphasise that extensive CE research in this area can further improve its performance. Of particular interest, developing specific CE algorithms for these filtered based systems will be a plus. Likewise, developing specific CE schemes for BFDM-OQAM transceivers is still an open area of research. BFDM is also a potential candidate for the upcoming xG wireless networks because of its peculiar pulse shapes. However, as earlier mentioned, only a few works have analysed the performance of CE schemes for BFDM-OQAM. Thus more research works can be actualised in this area in order for BFDM schemes to attain its full potential. Moreover, CE for f-OFDM systems (which is considered as a potential waveform candidate of xG networks) is an open area for future research, as the performance of CE methods for this waveform is not well researched and documented in the literature. To ensure excellence signal transmission and receptions when using f-OFDM as the underlying network waveform while primarily considering user QoS and QoE enhancement, adequate CE techniques for this waveform is required.

Additionally, as shown in the results presented in Section 5, we observe that the adaptive CE schemes perform better than the linear CE schemes for both the NPR and Non-PR conditions. This showcase the adaptive CE schemes as a better alternative to the linear CE schemes for FBMC systems, whereby researchers and practitioners in this field can easily make meaningful decisions based on their application requirements. However, as mentioned, the FBMC transceiver application requires specific CE algorithms for both waveform candidates considered in this paper, and other promising waveforms such as UFMC, BFDM, f-OFDM. More importantly, application specific CE algorithm is required for the FBMC transceiver because the studied CE schemes, both the adaptive and linear schemes, plummet when Non-PR condition is assumed. In reality, it is difficult to reconstruct a near perfect condition. This means we cannot eliminate error completely in real-time. Thus, the Non-PR condition is often the case in reality. This gives rise to the need for more sophisticated CE algorithms suitable for Non-PR condition. It is also observed from this study that CE is not well studied for NC-OFDM system. NC-OFDM systems offer higher data rates; as such, they are very useful in cognitive radio applications which are well designed to effectively manage and efficiently utilise the scarce available frequency spectrum for an eMBB communication system. Therefore, extensive CE research for NC-OFDM systems can further improve the quality of transmitted signal's reception as well as total system throughput over fading channels for enhancement in user QoE. It is worthy to mention that machine learning technologies can also be exploited as a possible research topic, where unsupervised software-based CE and prediction algorithms can be developed for estimating the frequency and time dispersion characteristics of the multipath fading channel in application to the above-mentioned waveform candidates of the 5G networks and beyond. For reference, refer to [153] Finally, massive MIMO systems (which adopt large-scale transmit antenna arrays) and other radio access techniques (such as RSMA, NOMA and SCMA) are pertinent technologies that form technical components of the upcoming 5G networks and beyond. Joint channel estimation, carrier frequency offset estimation and interference cancellation/decoding schemes are also useful techniques that can considerably enhance the throughput and spectral efficiency of these wireless communication systems. Consequently, developing novel algorithms that will jointly estimate the channel characteristics, the carrier frequency offset, as well as interference cancellation methods for

performance enhancement of the mentioned xG technologies is an open research direction for the emerging 5G networks and beyond.

7. Conclusions

This paper presents a review of the performances of CE schemes for candidate waveforms of xG wireless networks. Firstly, in Section 2, the design of digital filters is reviewed since the physical layer structure of these waveforms are based on filters developed from a well-designed prototype filter. In subsequent sections, the importance of CE for wireless communication networks is emphasised. As such, the CE techniques deployed for these waveforms in the literature are identified and classified, where the classification of CE schemes in application to filter and non-filter-based waveforms currently under consideration for xG networks is narrowed down. In addition, this paper summarises the performance comparison of CE schemes that are immensely considered as waveform candidates of xG networks. Finally, the performances of two linear CE schemes and three adaptive CE schemes for filter bank OFDM-OQAM and GFDM-OQAM based transceivers over slow and fast frequency selective Rayleigh fading channels are reviewed. The performance of these estimators is verified assuming NPR and Non-PR low-pass prototype filter design. It is observed from the simulation results presented in Section 5 that the adaptive CE schemes are more suitable as compared to the linear schemes for FBMC based transceivers. However, the need for more novel and application-specific CE schemes for FMBC transceivers is paramount, especially for Non-PR filter design. Thus, keeping in view the coverage of this review paper, we presumed that this paper will spring up possible research directions in improving the performances of the considered filter and non-filter based xG waveform candidates over frequency and dispersive time-varying Rayleigh fading channels.

Author Contributions: The review idea was conceived and implemented by O.E.I., O.O.O. and O.E.I. developed the structure of the review and write up the paper. O.O.O., A.D.F. and D.J.J.V. supervised the review presentation and the paper write up.

Funding: This research received no external funding.

Acknowledgments: The financial assistance of the National Research Foundation (NRF) towards this research is hereby acknowledged. Opinions expressed and conclusions arrived at are those of the authors and are not necessarily to be attributed to the NRF.

Conflicts of Interest: The authors declare no conflict of interest.

References

1. Jain, A.; Nagaria, D. Filter bank spectrum sensing for Cognitive Radio oriented wireless network. In Proceedings of the Conference on Communication, Control and Intelligent Systems (CCIS), Mathura, India, 7–8 November 2015; pp. 133–136.
2. Farhang-Boroujeny, B. Filter Bank Spectrum Sensing for Cognitive Radios. *IEEE Trans. Signal Process.* **2008**, 56, 1801–1811. [CrossRef]
3. Lajnef, H.; Dakhli, M.C.; Bouallegue, M.H.R. The Nonlinear Distortion cancellation for the effect of HPA nonlinearities in filter bank based multi-carrier (FBMC) for Cognitive Radio systems. In Proceedings of the Conference on Wireless Communications and Mobile Computing Conference (IWCMC), Paphos, Cyprus, 5–9 September 2016; pp. 638–643.
4. Akkarajitsakul, K.; Hossain, E.; Niyato, D.; Kim, D.I. Game Theoretic Approaches for Multiple Access in Wireless Networks: A Survey. *IEEE Commun. Surv. Tutor.* **2011**, 13, 372–395. [CrossRef]
5. Mitra, A. *Notes on Mobile Communication*; Department of Electronics and Communication Engineering, Indian Institute of Technology: Bangalore, India, 2009.
6. Hara, S.; Prasad, R. Overview of multicarrier CDMA. *IEEE Commun. Mag.* **1997**, 35, 126–133. [CrossRef]
7. Sun, S.; Han, S.; Yu, Q.; Meng, W.; Li, C. A survey of two kinds of complementary coded CDMA wireless communications. In Proceedings of the IEEE Global Communications Conference, Austin, TX, USA, 8–10 December 2014; pp. 468–472.

8. LaSorte, N.; Barnes, W.J.; Refai, H.H. The History of Orthogonal Frequency Division Multiplexing. In Proceedings of the IEEE Global Telecommunications Conference (GLOBECOM), New Orleans, LO, USA, 30 November–4 December 2008; pp. 1–5.
9. Mirahmadi, M.; Al-Dweik, A.; Shami, A. BER reduction of OFDM based broadband communication systems over multipath channels with impulsive noise. *Trans. Commun.* **2013**, *61*, 4602–4615. [CrossRef]
10. Fang, J.; You, Z.; Lu, I.T.; Li, J.; Yang, R. Comparisons of filter bank multicarrier systems. In Proceedings of the IEEE Long Island Systems, Applications and Technology Conference (LISAT), Farmingdale, NY, USA, 3–3 May 2013; pp. 1–6.
11. Cui, W.; Qu, D.; Jiang, T.; Farhang-Boroujeny, B. Coded Auxiliary Pilots for Channel Estimation in FBMC-OQAM Systems. *Trans. Veh. Technol.* **2016**, *65*, 2936–2946. [CrossRef]
12. Nam, H.; Choi, M.; Han, S.; Kim, C.; Choi, S.; Hong, D. A New Filter-Bank Multicarrier System with Two Prototype Filters for QAM Symbols Transmission and Reception. *IEEE Trans. Wirel. Commun.* **2016**, *15*, 5998–6009. [CrossRef]
13. Vakilian, V.; Wild, T.; Schaich, F.; ten Brink, S.; Frigon, J.F. Universal-filtered multi-carrier technique for wireless systems beyond LTE. In Proceedings of the IEEE Globecom Workshops (GC Workshops), Atlanta, GA, USA, 9–13 December 2013; pp. 223–228.
14. Jafri, A.R.; Majid, J.; Shami, M.A.; Imran, M.A.; Najam-Ul-Islam, M. Hardware Complexity Reduction in Universal Filtered Multicarrier Transmitter Implementation. *IEEE Access* **2017**, *5*, 13401–13408. [CrossRef]
15. Ayadi, R.; Siala, M.; Kammoun, I. Transmit/receive pulse-shaping design in BFDM systems over time-frequency dispersive AWGN channel. In Proceedings of the IEEE Conference on Signal Processing and Communications (ICSPC), Dubai, UAE, 24–27 November 2007; pp. 772–775.
16. Siclet, C.; Siohan, P. Design of BFDM/OQAM systems based on biorthogonal modulated filter banks. In Proceedings of the IEEE Global Telecommunications Conference (GLOBECOM), San Francisco, CA, USA, 27 November–1 December 2000; pp. 701–705.
17. Gaspar, D.; Mendes, L.; Pimenta, T. GFDM BER Under Synchronization Errors. *Commun. Lett.* **2017**, *21*, 1743–1746. [CrossRef]
18. Lim, B.; Ko, Y.C. SIR Analysis of OFDM and GFDM Waveforms with Timing Offset, CFO and Phase Noise. *Trans. Wirel. Commun.* **2017**, *16*, 6979–6990. [CrossRef]
19. Rana, M.M. An adaptive channel estimation technique for OFDM based cognitive radio systems. In Proceedings of the Conference on Computer and Information Technology (ICCIT), Dhaka, Bangladesh, 22–24 December 2011; pp. 315–320.
20. Zhao, Z.; Cheng, X.; Wen, M.; Jiao, B.; Wang, C. Channel Estimation Schemes for IEEE 802.11p Standard. *IEEE Intell. Transp. Syst. Mag.* **2013**, *5*, 38–49. [CrossRef]
21. Ogundile, O.O.; Versfeld, D.J.J. Iterative Channel Estimation and Symbol Level Reed-Solomon Decoding Receivers for OFDM Systems. *IEICE Trans. Commun.* **2017**, *E100-B*, 500–508. [CrossRef]
22. Velamala, H. Filter Bank Multicarrier Modulation for Spectrally Agile Waveform Design. Ph.D. Thesis, Department Electrical & Computer Engineering, Worcester Polytechnic Institute, Worcester, MA, USA, 2013.
23. Kuc, R. *Introduction to Digital Signal Processing*; McGraw-Hill: New York, NY, USA, 1988.
24. Crochiere, R.E.; Rabiner, L.R. Interpolation and decimation of digital signals—A tutorial review. *Proc. IEEE* **1981**, *69*, 300–331. [CrossRef]
25. Proakis, J.G.; Manolakis, D.G. *Digital Signal Processing*; Prentice-Hall Inc.: Upper Saddle River, NJ, USA, 1996.
26. Kumar, R.; Kumar, A.; Singh, S.P. A review on decade of multi-rate filters. In Proceedings of the Conference on Electronics and Communication Systems (ICECS), Coimbatore, India, 26–27 February 2015; pp. 1615–1620.
27. Vaidyanathan, P. P. Multirate digital filters, filter banks, polyphase networks, and applications: A tutorial. *Proc. IEEE* **1990**, *78*, 56–93. [CrossRef]
28. Shynk, J.J. Frequency-domain and multirate adaptive filtering. *IEEE Signal Process. Mag.* **1992**, *9*, 14–37. [CrossRef]
29. Meyer, R.; Burrus, C. Design and implementation of multirate digital filters. *IEEE Trans. Acoust. Speech Signal Process.* **1976**, *24*, 53–58. [CrossRef]
30. Shenoy, R.G.; Burnside, D.; Parks, T.W. Linear periodic systems and multirate filter design. *IEEE Trans. Signal Processing*, **1994**, *42*, 2242–2256. [CrossRef]

31. Farhang-Boroujeny, B. Filter Bank Multicarrier Modulation: A Waveform Candidate for 5G and Beyond. *Hindawi Adv. Electr. Eng.* **2014**, *2014*, 1–25. [CrossRef]
32. Martin, K.W. Small side-lobe filter design for multitone data-communication applications. *IEEE Trans. Circuits Syst. II Analog Digit. Signal Process.* **1998**, *45*, 1155–1161. [CrossRef]
33. Zhou, D. *A Review of Polyphase Filter Banks and Their Application*; In-House final technical report—Air Force Research Laboratory: New York, NY, USA, 2006; pp. 1–29.
34. Zahradnik, P.; Vlcek, M. Perfect decomposition narrow-band FIR filter banks. *IEEE Trans. Circuits Syst. II Express Briefs* **2012**, *59*, 805–809. [CrossRef]
35. Vetterli, M. A theory of multirate filter banks. *IEEE Trans. Acoust. Speech Signal Process.* **1987**, *35*, 356–372. [CrossRef]
36. Diniz, L.R.; Netto, S.L. Design of high-resolution cosine-modulated transmultiplexers with sharp transition band. *IEEE Trans. Signal Process.* **2004**, *52*, pp. 1278 – 1288. [CrossRef]
37. Michailow, N.; Matthé, M.; Gaspar, I.S.; Caldevilla, A.N.; Mendes, L.L.; Festag, A.; Fettweis, G. Generalized frequency division multiplexing for 5th generation cellular networks. *IEEE Trans. Commun.* **2014**, 62, 3045–3061. [CrossRef]
38. Farhang-Boroujeny, B.; Lin, L. Cosine modulated multitone for very high-speed digital subscriber lines. In Proceedings of the IEEE Conference on Acoustics, Speech, and Signal Processing Proceedings (ICASSP), Philadelphia, PA, USA, 23–23 March 2005; pp. 345–348.
39. Lakshmanan, M.K.; Nikookar, H. A Review of Wavelets for Digital Wireless Communication. *Int. J. Wirel. Pers. Commun.* **2006**, *37*, 387–420. [CrossRef]
40. Sandberg, S.D.; Tzannes, M.A. Overlapped discrete multitone modulation for high speed copper wire communications. *IEEE J. Sel. Areas Commun.* **1995**, *13*, 1571–1585. [CrossRef]
41. Alhava, J.; Renfors, M. Exponentially-modulated filter bank transmultiplexer with fine-coarse adaptive filtering. In Proceedings of the International Symposium on Communications, Control and Signal Processing (ISCCSP), St Julians, Malta, 12–14 March 2008; pp. 68–72.
42. Lin, L.; Farhang-Boroujeny, B. Convergence analysis of blind equalizer in a filter-bank-based multicarrier communication system. *IEEE Trans. Signal Process.* **2006**, *54*, 4061–4067. [CrossRef]
43. Farhang-Boroujeny, B.; Lin, L. Analysis of post-combiner equalizers in cosine-modulated filterbank-based transmultiplexer systems. *IEEE Trans. Signal Process.* **2003**, *51*, 3249–3262. [CrossRef]
44. Mirabbasi, S.; Martin, K. Overlapped complex-modulated transmultiplexer filters with simplified design and superior stopbands. *IEEE Trans. Circuits Syst. II Analog Digital Signal Process.* **2003**, *50*, 456–469. [CrossRef]
45. Alhava, J.; Viholainen, A.; Renfors, M. Efficient implementation of complex exponentially-modulated filter banks. In Proceedings of the International Symposium on Circuits and Systems (ISCAS), Bangkok, Thailand, 25–28 May 2003; pp. 157–160.
46. Evans, D. *The Internet of Things: How the Next Evolution of the Internet is Changing Everything*; Cisco White Paper; Cisco Internet Business Solutions Group (IBSG): San Jose, CA, USA, 2011; p. 1.
47. Roessler, A. 5G Waveform Candidates. Available online: https://scdn.rohde-schwarz.com/ur/pws/dl_downloads/dl_application/application_notes/1ma271/1MA271_0e_5G_waveform_candidates.pdf (accessed on 14 January 2019).
48. Sahni, V.D.; Kumar, N.; Saxena, V.N. Novel hybrid technique(s) for PAPR reduction in OFDM systems. In Proceedings of the Conference on Signal Processing and Communication (ICSC), Noida, India, 26–28 Decemebr 2016; pp. 512–515.
49. Lim, D.W.; Heo, S.J.; No, J.S. An overview of peak-to-average power ratio reduction schemes for OFDM signals. *J. Commun. Netw.* **2009**, *11*, 229–239. [CrossRef]
50. Ehsanfar, S.; Matthe, M.; Zhang, D.; Fettweis, G. Theoretical Analysis and CRLB Evaluation for Pilot-Aided Channel Estimation in GFDM. In Proceedings of the IEEE Global Communications Conference (GLOBECOM), Washington, DC, USA, 4–8 December 2016; pp. 1–7.
51. Ehsanfar, S.; Matthe, M.; Zhang, D.; Fettweis, G. Interference-Free Pilots Insertion for MIMO-GFDM Channel Estimation. In Proceedings of the IEEE Wireless Communications and Networking Conference (WCNC), San Francisco, CA, USA, 19–22 March 2017; pp. 1–6.
52. Ehsanfar, S.; Matthe, M.; Zhang, D.; Fettweis, G. A Study of Pilot-Aided Channel Estimation in MIMO-GFDM Systems. In Proceedings of the International ITG Workshop on Smart Antennas (WSA), Munich, Germany, 9–11 March 2016; pp. 1–8.

53. Chang, H.L.; Tsai, M.H. Optimistic DRX for Machine-Type Communications in LTE-A Network. *IEEE Access* **2018**, *6*, 9887–9897. [CrossRef]
54. Li, Y.; Sun, K.; Cai, L. Cooperative Device-to-Device Communication With Network Coding for Machine Type Communication Devices. *IEEE Trans. Wirel. Commun.* **2018**, *17*, 296–309. [CrossRef]
55. Cheng, R.G.; Becvar, Z.; Yang, P.H. Modeling of Distributed Queueing-Based Random Access for Machine Type Communications in Mobile Networks. *IEEE Commun. Lett.* **2018**, *22*, 129–132. [CrossRef]
56. Akpakwu, G.A.; Silva, B.J.; Hancke, G.P.; Abu-Mahfouz, A.M. A Survey on 5G Networks for the Internet of Things: Communication Technologies and Challenges. *IEEE Access* **2018**, *6*, 3619–3647. [CrossRef]
57. Ji, H.; Park, S.; Yeo, J.; Kim, Y.; Lee, J.; Shim, B. Ultra-Reliable and Low-Latency Communications in 5G Downlink: Physical Layer Aspects. *IEEE Wirel. Commun.* **2018**, *25*, 124–130. [CrossRef]
58. Liu, C.F.; Bennis, M. Ultra-Reliable and Low-Latency Vehicular Transmission: An Extreme Value Theory Approach. *IEEE Commun. Lett.* **2018**, *22*, 1292–1295. [CrossRef]
59. Zhang, K.; Leng, S.; He, Y.; Maharjan, S.; Zhang, Y. Mobile Edge Computing and Networking for Green and Low-Latency Internet of Things. *IEEE Commun. Mag.* **2018**, *56*, 39–45. [CrossRef]
60. Abu-Lebdeh, M.; Sahoo, J.; Glitho, R.; Tchouati, C.W. Cloudifying the 3GPP IP multimedia subsystem for 4G and beyond: A survey. *IEEE Commun. Mag.* **2016**, *54*, 91–97. [CrossRef]
61. Ijaz, A.; Zhang, L.; Xiao, P.; Tafazolli, R. *Analysis of Candidate Waveforms for 5G Cellular Systems. Towards 5G Wireless Networks: Chapter 1*; Intech Open: London, UK, 2016; pp. 1–25.
62. Nguyen, T.M.; Ajib, W.; Assi, C. A Novel Cooperative Non-Orthogonal Multiple Access (NOMA) in Wireless Backhaul Two-Tier HetNets. *IEEE Trans. Wirel. Commun.* **2018**, *17*, 4873–4887. [CrossRef]
63. Ni, D.; Hao, L.; Tran, Q.T.; Qian, X. Power Allocation for Downlink NOMA Heterogeneous Networks. *IEEE Access* **2018**, *6*, 26742–26752. [CrossRef]
64. Fu, Y.; Hong, Y.; Chen, L.K.; Sung, C.W. Enhanced Power Allocation for Sum Rate Maximization in OFDM-NOMA VLC Systems. *IEEE Photonics Technol. Lett.* **2018**, *30*, 1218–1221. [CrossRef]
65. Zhang, H.; Qiu, Y.; Long, K.; Karagiannidis, G.K.; Wang, X.; Nallanathan, A. Resource Allocation in NOMA-Based Fog Radio Access Networks. *IEEE Wirel. Commun.* **2018**, *25*, 110–115. [CrossRef]
66. Richardson, T.; Kudekar, S. Design of Low-Density Parity Check Codes for 5G New Radio. *IEEE Commun. Mag.* **2018**, *56*, 28–34. [CrossRef]
67. Wu, X.; Jiang, M.; Zhao, C.; Ma, L.; Wei, Y. Low-Rate PBRL-LDPC Codes for URLLC in 5G. *IEEE Wirel. Commun. Lett.* **2017**, *21*, 1–4. [CrossRef]
68. Bellili, F.; Methenni, A.; Amor, S.B.; Affes, S.; Stèphenne, A. Time Synchronization of Turbo-Coded Square-QAM-Modulated Transmissions: Code-Aided ML Estimator and Closed-Form Cramér–Rao Lower Bounds. *IEEE Trans. Veh. Technol.* **2017**, *66*, 10776–10792. [CrossRef]
69. Ahn, B.; Yoon, S.; Heo, J. Low Complexity Syndrome-Based Decoding Algorithm Applied to Block Turbo Codes. *IEEE Access* **2018**, *6*, 26693–26706. [CrossRef]
70. İşcan, O.; Xu, W. Window-Interleaved Turbo Codes. *IEEE Commun. Lett.* **2018**, *22*, 676–679. [CrossRef]
71. Dai, J.; Niu, K.; Si, Z.; Dong, C.; Lin, J. Polar-Coded Non-Orthogonal Multiple Access. *IEEE Trans. Signal Process.* **2018**, *66*, 1374–1389. [CrossRef]
72. Gerzaguet, R.; Kténas, D.; Cassiau, N.; Doré, J.B. Comparative study of 5G waveform candidates for below 6 GHz air interface. In Proceedings of the ETSI Workshop on Future Radio Technologies-Air Interface, Sophia Antipolis, France, 27–28 January 2016; pp. 1–9.
73. Coleri, S.; Ergen, M.; Puri, A.; Bahai, A. Channel estimation techniques based on pilot arrangement in OFDM systems. *IEEE Trans. Broadcast.* **2002**, *48*, 223–229. [CrossRef]
74. Almoneer, M.; Rohde, C.; Hassan, K.; Gerstacker, W.H. Intercarrier Interference-Aware Pilot-Aided Channel Estimation in OFDM Systems. *IEEE Trans. Broadcast.* **2017**, *63*, 449–462. [CrossRef]
75. Idris, A.; Farhana, A.N.; Adiba, H.; Kassim, M. BER and PAPR analysis of MIMO OFDMA and SCFDMA system using different diversity techniques. In Proceedings of the IEEE Conference on Control System, Computing and Engineering (ICCSCE), Penang, Malaysia, 24–26 November 2017; pp. 293–298.
76. Zhang, X.; Jia, M.; Chen, L.; Ma, J.; Qiu, J. Filtered-OFDM–Enabler for Flexible Waveform in the 5th Generation Cellular Networks. In Proceedings of the IEEE Global Communications Conference (GLOBECOM), San Diego, CA, USA, 6–10 December 2015; pp. 1–6.

77. Wu, D.; Zhang, X.; Qiu, J.; Gu, L.; Saito, Y.; Benjebbour, A.; Kishiyama, Y. A Field Trial of f-OFDM toward 5G. In Proceedings of the IEEE Globecom Workshops (GC Wkshps), Washington, DC, USA, 4–8 December 2016; pp. 1–6.
78. Zhang, L.; Ijaz, A.; Xiao, P.; Molu, M.M.; Tafazolli, R. Filtered OFDM Systems, Algorithms, and Performance Analysis for 5G and Beyond. *IEEE Trans. Commun.* **2018**, *66*, 1205–1218. [CrossRef]
79. Zhang, X. Design of FIR Halfband Filters for Orthonormal Wavelets Using Remez Exchange Algorithm. *IEEE Signal Process. Lett.* **2009**, *16*, 814–817. [CrossRef]
80. Chen, L.; Yu, J.G. Interference cancelation scheme with variable bandwidth allocation for universal filtered multicarrier systems in 5G networks. *EURASIP J. Wirel. Commun. Netw.* **2018**, *2018*, 1–10. [CrossRef]
81. Poornima, T.; Dhinesh, K.; Sudhakar, R. Waveform candidates for 5G mobile communications. In Proceedings of the IEEE Conference on Recent Trends in Electronics, Information & Communication Technology (RTEICT), Bangalore, India, 19–20 May 2017; pp. 856–860.
82. Desta, Y.T.; Tao, J.; Zhang, W. Review on Selected Channel Estimation Algorithms for Orthogonal Frequency Division Multiplexing System. *Inf. Technol. J.* **2011**, *10*, 914–926. [CrossRef]
83. Balogun, B.M. Frequency Synchronization in Multiuser OFDM-IDMA Systems. Ph.D. Thesis, Department of Electrical Engineering, & Computer Engineering, University of Kwazulu-Natal, Durban, South Africa, 2013.
84. Ijiga, O.E. Channel Estimation Techniques for Filter Bank Multicarrier Based Transceivers for Next Generation of Wireless Networks. Ph.D. Thesis, School of Election & Information Engineering, University of the Witwatersrand, Johannesburg, South Africa, 2017.
85. Ogundile, O.O.; Oyerinde, O.O.; Versfeld, D.J.J. Decision directed iterative channel estimation and Reed Solomon decoding over flat fading channels. *IET Commun.* **2015**, *9*, 2077–2084. [CrossRef]
86. Van de Beek, J.-J.; Edfors, O.; Sandell, M.; Wilson, S.K.; Borjesson, P.O. On channel estimation in OFDM systems. In Proceedings of the IEEE Vehicular Technology Conference, Chicago, IL, USA, 25–28 July 1995; pp. 815–819.
87. James, A.R.; Benjamin, R.S.; John, S.; Joseph, T.M.; Mathai, V.; Pillai, S.S. Channel estimation for OFDM systems. In Proceedings of the Conference on Signal Processing, Communication, Computing and Networking Technologies, Thuckafay, India, 21–22 July 2011; pp. 587–591.
88. Morelli, M.; Mengali, U. A comparison of pilot-aided channel estimation methods for OFDM systems. *IEEE Trans. Signal Process.* **2001**, *49*, 3065–3073. [CrossRef]
89. Kong, D.; Xia, X.G.; Jiang, T.; Gao, X. Channel Estimation in CP-OQAM-OFDM Systems. *IEEE Trans. Signal Process.* **2014**, 62, pp. 5775-5786. [CrossRef]
90. Ogundile, O.O.; Versfeld, D.J.J. A Low Complexity Iterative Channel Estimation and Decoding Receiver Based on Reed-Solomon PTA. *IEEE Access* **2016**, *4*, 8805–8813. [CrossRef]
91. Park, S.; Shim, B.; Choi, J.W. Iterative Channel Estimation Using Virtual Pilot Signals for MIMO-OFDM Systems. *IEEE Trans. Signal Process* **2015**, *63*, 3032–3045. [CrossRef]
92. Ozdemir, M.K.; Arslan, H. Channel estimation for wireless ofdm systems. *IEEE Commun. Surv. Tutor.* **2007**, *9*, 18–48. [CrossRef]
93. Yoo, D.S.; Lim, J. MSE expression for transform-based decision-directed channel estimation schemes in *M*-PSK OFDM systems. *Electron. Lett.* **2016**, *52*, 363–365. [CrossRef]
94. Park, S.; Choi, J.W.; Lee, K.; Shim, B. Soft decision-directed channel estimation for multiuser MIMO systems. In Proceedings of the IEEE Symposium on Personal, Indoor, and Mobile Radio Communications (PIMRC), Hong Kong, China, 30 August–2 September 2015; pp. 95–99.
95. Tseng, C.H.; Cheng, Y.C.; Chung, C.D. Subspace-Based Blind Channel Estimation for OFDM by Exploiting Cyclic Prefix. *IEEE Wirel. Commun. Lett.* **2013**, *2*, 691–694. [CrossRef]
96. Mawatwal, K.; Sen, D.; Roy, R. A Semi-Blind Channel Estimation Algorithm for Massive MIMO Systems. *IEEE Wirel. Commun. Lett.* **2017**, *6*, 70–73. [CrossRef]
97. Chang, T.H.; Ma, W.K.; Chi, C.Y. Maximum-Likelihood Detection of Orthogonal Space-Time Block Coded OFDM in Unknown Block Fading Channels. *IEEE Trans. Signal Process.* **2008**, *56*, 1637–1649. [CrossRef]
98. Wang, M.L.; Li, C.P.; Huang, W.J. Semi-Blind Channel Estimation and Precoding Scheme in Two-Way Multi-Relay Networks. *IEEE Trans. Signal Process.* **2017**, *65*, 2576–2587. [CrossRef]
99. Ban, Y.; Hu, Q.; Mao, Z.; Zhao, Z. Semi-blind pilot-aided channel estimation in uplink cloud radio access networks. *China Commun.* **2016**, *13*, 72–79. [CrossRef]

100. Zhang, S.; Wang, J.; Li, S. A channel estimation method for NC-OFDM systems in cognitive radio context. In Proceedings of the IEEE Singapore International Conference on Communication Systems (ICCS), Guangzhou, China, 19–21 Novemebr 2008; pp. 208–212.
101. Min, J.; Xue-mai, G.; Qun, W. An improved channel estimation method for NC-OFDM systems in Cognitive Radio context. In Proceedings of the Conference on Communications and Networking in China (CHINACOM), Harbin, China, 17–19 August 2011; pp. 147–150.
102. Zhu, C.; Yang, S. The Interference Constrained Pilot Design for NC-OFDM Systems in Cognitive Radios. In Proceedings of the Conference on Wireless Communications, Networking and Mobile Computing (WiCOM), Shanghai, China, 21–23 September 2012; pp. 1–4.
103. Liu, J.; Feng, S.; Wang, H. Comb-Type Pilot Aided Channel Estimation in Non-Contiguous OFDM Systems for Cognitive Radio. In Proceedings of the Conference on Wireless Communications, Networking and Mobile Computing (WiCom), Beijing, China, 24–26 September 2009; pp. 1–4.
104. Zhang, Y.; Xu, X.; Chen, B.; Dai, X. A suboptimal pilot design for NC-OFDM systems. In Proceedings of the IEEE Conference on Communication Technology (ICCT), Nanjing, China, 11–14 November 2010; pp. 801–804.
105. Manasseh, E.; Ohno, S.; Nakamoto, M. Pilot design for non-contiguous spectrum usage in OFDM-based cognitive radio networks. In Proceedings of the European Signal Processing Conference (EUSIPCO), Bucharest, Romania, 27–31 August 2012; pp. 465–469.
106. Berger, C.R.; Wang, Z.; Huang, J.; Zhou, S. Application of compressive sensing to sparse channel estimation. *IEEE Commun. Mag.* **2010**, *48*, 164–174. [CrossRef]
107. Jia, M.; Liu, X.; Gu, X. Channel estimation algorithm based on compressive sensing for NC-OFDM systems in cognitive radio context. *Int. J. Adv. Comput. Technol. (IJACT)* **2013**, *5*, pp. 343–351.
108. Chen, E.; Chu, C. Channel estimation for NC-OFDM systems based on subspace pursuit algorithm. In Proceedings of the IEEE Conference on Signal Processing (ICSP), Beijing, China, 21–25 October 2012; pp. 88–91.
109. Huang, S.; Lin, J.; Chou, K. Novel Channel Estimation Techniques on SC-FDMA Uplink Transmission. In Proceedings of the IEEE Vehicular Technology Conference, Taipei, Taiwan, 16–19 May 2010; pp. 1–5.
110. Luan, Y.; Kan, C.; Du, H.; Zhao, Q. An improved LS channel estimation algorithm of SC-FDMA. In Proceedings of the IEEE Conference on Anti-counterfeiting, Security, and Identification (ASID), Xiamen, China, 25–27 September 2015; pp. 128–131.
111. Jin, X. Channel Estimation Techniques of SC-FDMA. Ph.D. Thesis, Karlstad University, Karlstad, Sweden, 2007.
112. Mongol, B.; Yamazato, T.; Okada, H.; Katayama, M. Channel Estimation for BFDM/OQAM System in Dispersive Time-Varying Channels. In Proceedings of the International Symposium on Wireless Communication Systems, Valencia, Spain, 6–8 September 2006; pp. 159–163.
113. Wang, X.; Wild, T.; Schaich, F.; ten Brink, S. Pilot-Aided Channel Estimation for Universal Filtered Multi-Carrier. In Proceedings of the IEEE Vehicular Technology Conference (VTC2015-Fall), Boston, MA, USA, 6–9 September 2015; pp. 1–5.
114. Qi, C.; Wu, L. A hybrid compressed sensing algorithm for sparse channel estimation in MIMO OFDM systems. In Proceedings of the IEEE Conference on Acoustics, Speech and Signal Processing (ICASSP), Prague, Czech Republic, 22–27 May 2011; pp. 3488–3491.
115. Baltar, L.G.; Mezghani, A.; Nossek, J.A. Spectral efficient channel estimation algorithms for FBMC/OQAM systems: A comparison. In Proceedings of the International Symposium on Wireless Communications Systems (ISWCS), Barcelona, Spain, 26–29 August 2014; pp. 707–711.
116. Kwon, B.; Kim, S.; Jeon, D.; Lee, S. Iterative Interference Cancellation and Channel Estimation in Evolved Multimedia Broadcast Multicast System Using Filter-Bank Multicarrier-Quadrature Amplitude Modulation. *IEEE Trans. Broadcast.* **2016**, *62*, 864–875. [CrossRef]
117. Fuhrwerk, M.; Moghaddamnia, S.; Peissig, J. Scattered Pilot-Based Channel Estimation for Channel Adaptive FBMC-OQAM Systems. *IEEE Trans. Wirel. Commun.* **2017**, *16*, 1687–1702. [CrossRef]
118. Lélé, C.; Javaudin, J.P.; Legouable, R.; Skrzypczak, A.; Siohan, P. Channel estimation methods for preamble-based OFDM/OQAM modulations. *Eur. Trans. Telecommun.* **2008**, *19*, 741–750. [CrossRef]

119. Kofidis, E.; Katselis, D. Improved interference approximation method for preamble-based channel estimation in FBMC/OQAM. In Proceedings of the European Signal Processing Conference, Barcelona, Spain, 29 August–2 September 2011; pp. 1603–1607.
120. Kofidis, E. Short preamble-based estimation of highly frequency selective channels in FBMC/OQAM. In Proceedings of the Conference on Acoustics, Speech and Signal Processing (ICASSP), Florence, Italy, 4–9 May 2014; pp. 8058–8062.
121. Zhao, Z.; Vucic, N.; Schellmann, M. A simplified scattered pilot for FBMC/OQAM in highly frequency selective channels. In Proceedings of the International Symposium on Wireless Communications Systems (ISWCS), Barcelona, Spain, 26–29 August 2014; pp. 819–823.
122. Baltar, L.G.; Mezghani, A.; Nossek, J.A. EM based per-subcarrier ML channel estimation for filter bank multicarrier systems. In Proceedings of the International Symposium on Wireless Communication Systems (ISWCS), Ilmenau, Germany, 27–30 August 2013; pp. 1–5.
123. Aldababseh, M.; Jamoos, A. Estimation of FBMC/OQAM fading channels using dual Kalman filters. *Sci. World J.* **2014**, *2014*, 1–9. [CrossRef]
124. Tang, N.; He, S.; Wang, H.; Huang, Y.; Yang, L. Training sequence design for channel estimation and IQ imbalance compensation in GFDM systems. In Proceedings of the International Conference on Wireless Communications and Signal Processing (WCSP), Nanjing, China, 11–13 October 2017; pp. 1–6.
125. Zhang, J.; Li, Y.; Niu, K. Iterative channel estimation algorithm based on compressive sensing for GFDM. In Proceedings of the IEEE Conference on Network Infrastructure and Digital Content (IC-NIDC), Beijing, China, 23–25 September 2016; pp. 244–248.
126. Vilaipornsawai, U.; Jia, M. Scattered-pilot channel estimation for GFDM. In Proceedings of the IEEE Wireless Communications and Networking Conference (WCNC), Istanbul, Turkey, 6–9 April 2014; pp. 1053–1058.
127. Niazadeh, R.; Babaie-Zadeh, M.; Jutten, C. On the Achievability of Cramér–Rao Bound in Noisy Compressed Sensing. *IEEE Trans. Signal Process.* **2012**, *60*, 518–526. [CrossRef]
128. Zakaria, R.; Le Ruyet, D. A novel filter-bank multicarrier scheme to mitigate the intrinsic interference: application to MIMO systems. *IEEE Trans. Wirel. Commun.* **2012**, *11*, 1112–1123. [CrossRef]
129. Tensubam, B.D.; Singh, S. A review on FBMC: An efficient multicarrier modulation system. *Int. J. Comput. Appl.* **2014**, *98*, 6–9.
130. Danneberg, M.; Michailow, N.; Gaspar, I.; Zhang, D.; Fettweis, G. Flexible GFDM Implementation in FPGA with Support to Run-Time Reconfiguration. In Proceedings of the IEEE Vehicular Technology Conference, VTC Fall 2015, Boston, MA, USA, 6–9 September 2015; pp. 1–2.
131. Viholainen, A.; Ihalainen, T.; Stitz, T.H.; Renfors, M.; Bellanger, M. Prototype filter design for filter bank based multicarrier transmission. In Proceedings of the European Signal Processing Conference, Glasgow, UK, 24–28 August 2009; pp. 1359–1363.
132. Masson, J.; Picel, Z. Flexible design of computationally efficient nearly perfect QMF filter banks. In Proceedings of the IEEE Conference on Acoustics, Speech, and Signal Processing (ICASSP), Tampa, FL, USA, 26–29 April 1985; pp. 541–544.
133. Saideh, M.; Berbineau, M.; Dayoub, I. On the Performance of Sliding Window TD-LMMSE Channel Estimation for 5G Waveforms in High Mobility Scenario. *IEEE Trans. Veh. Technol.* **2018**, *67*, 8974–8977. [CrossRef]
134. Ihalainen, T.; Viholainen, A.; Stitz, T.H.; Renfors, M. Generation of filter bank-based multicarrier waveform using partial synthesis and time domain interpolation. *IEEE Trans. Circuits Syst. I Regul. Papers* **2010**, *57*, 1767–1778. [CrossRef]
135. Baddour, K.E.; Beaulieu, N.C. Autoregressive modeling for fading channel simulation. *Trans. Wirel. Commun.* **2005**, *4*, 1650–1662. [CrossRef]
136. Haykin, S. *Adaptive Filter Theory*; Prentice Hall: Upper Saddle River, NJ, USA, 1986.
137. Scharf, L.L. *Statistical Signal Processing: Detection, Estimation and Time Series Analysis*; Addison-Wesley: Boston, MA, USA, 1991.
138. Ghosh, M.; Srinivasarao, C.; Sahoo, H.K. Adaptive channel estimation in MIMO-OFDM for indoor and outdoor environments. In Proceedings of the Conference on Wireless Communications, Signal Processing and Networking (WiSPNET), Chennai, India, 22–24 March 2017; pp. 2743–2747.
139. Rana, M.M.; Kim, J. LMS based blind channel estimation of SC-FDMA systems using variable step size and phase information. *Electron. Lett.* **2011**, *47*, 346–348. [CrossRef]

140. Beena, A.O.; Pillai, S.S.; Vijayakumar, N. An Adaptive Sparse Channel Estimation algorithm with fast convergence for broad band MIMO-OFDM systems. In Proceedings of the IEEE Conference on Circuits and Systems (ICCS), Thiruvananthapuram, India, 20–21 December 2017; pp. 151–156.
141. Rana, M.M. Performance comparison of LMS and RLS channel estimation algorithms for 4G MIMO OFDM systems. In Proceedings of the International Conference on Computer and Information Technology (ICCIT), Dhaka, Bangladesh, 22–24 December 2011; pp. 635–639.
142. Chang, L.; Li, G.Y.; Li, J.; Li, R. Blind parameter estimation of GFDM signals over frequency-selective fading channels. *IEEE Trans. Commun.* **2016**, *64*, 1120–1131. [CrossRef]
143. Michailow, N.; Mendes, L.; Matthé, M.; Gaspar, I.; Festag, A.; Fettweis, G. Robust WHT-GFDM for the Next Generation of Wireless Networks. *IEEE Commun. Lett.* **2015**, *19*, 106–109. [CrossRef]
144. Farhang, A.; Marchetti, N.; Doyle, L.E. Low-Complexity Modem Design for GFDM. *IEEE Trans. Signal Process.* **2016**, *64*, 1507–1518. [CrossRef]
145. Farhang, A.; Marchetti, N.; Doyle, L.E. Low complexity GFDM receiver design: A new approach. In Proceedings of the IEEE International Conference on Communications (ICC), London, UK, 8–12 June 2015; pp. 4775–4780.
146. Farhang-Boroujeny, B.; Moradi, H. Derivation of GFDM based on OFDM principles. In Proceedings of the IEEE Conference on Communications (ICC), London, UK, 8–12 June 2015; pp. 2680–2685.
147. Wang, P.S.; Lin, D.W. Maximum-likelihood blind synchronization for GFDM systems. *IEEE Signal Process. Lett.* **2016**, *23*, 790–794. [CrossRef]
148. Matthe, M.; Gaspar, I.; Zhang, D.; Fettweis, G. Reduced complexity calculation of LMMSE filter coefficients for GFDM. In Proceedings of the IEEE Vehicular Technology Conference, VTC F, Boston, MA, USA, 6–9 September 2015; pp. 1–2.
149. Minn, H.; Al-Dhahir, N. Optimal training signals for MIMO OFDM channel estimation. *IEEE Trans. Wirel. Commun.* **2006**, *5*, 1158–1168. [CrossRef]
150. Bandari, S.K.; Mani, V.V.; Drosopoulos, A. OQAM implementation of GFDM. In Proceedings of the International Conference on Telecommunications (ICT), Thessaloniki, Greece, 16–18 May 2016; pp. 1–5.
151. Akyildiz, I.F.; Lee, W.-Y.; Vuran, M.C.; Mohanty, S. NeXt generation/dynamic spectrum access/cognitive radio wireless networks: A survey. *J. Comput. Netw.* **2006**, *50*, 2127–2159. [CrossRef]
152. Schafhuber, D.; Matz, G. MMSE and adaptive prediction of time-varying channels for OFDM systems. *IEEE Trans. Wirel. Commun.* **2005**, *4*, 593–602. [CrossRef]
153. Motade, S.N.; Kulkarni, A.V. Channel Estimation and Data Detection Using Machine Learning for MIMO 5G Communication Systems in Fading Channel. *MDPI Technol.* **2018**, *6*, 1–16. [CrossRef]



© 2019 by the authors. Licensee MDPI, Basel, Switzerland. This article is an open access article distributed under the terms and conditions of the Creative Commons Attribution (CC BY) license (http://creativecommons.org/licenses/by/4.0/).